

Review

Plasma electrolysis for surface engineering

A.L. Yerokhin ^a, X. Nie ^b, A. Leyland ^b, A. Matthews ^{b,*}, S.J. Dowey ^c

^a Tula State University, 92, Lenin Avenue, 300600 Tula, Russia

^b Research Centre in Surface Engineering, University of Hull, Hull HU6 7RX, UK

^c Ion Coat Ltd, PO Box 53, Hull HU6 7TW, UK

Received 9 April 1999; accepted in revised form 23 July 1999

Abstract

This paper overviews the relatively new surface engineering discipline of plasma electrolysis, the main derivative of this being plasma electrolytic deposition (PED), which includes techniques such as plasma electrolytic oxidation (PEO) and plasma electrolytic saturation (PES) processes such as plasma electrolytic nitriding/carburizing (PEN/PEC). In PED technology, spark or arc plasma micro-discharges in an aqueous solution are utilised to ionise gaseous media from the solution such that complex compounds are synthesised on the metal surface through the plasma chemical interactions. The physical and chemical fundamentals of plasma electrolysis are discussed here. The equipment and deposition procedures for coating production are described, and the effects of electrolyte composition and temperature on ignition voltage, discharge intensity and deposited layer thickness and composition are outlined. AC-pulse PEO treatment of aluminium in a suitable passivating electrolyte allows the formation of relatively thick (up to 500 µm) and hard (up to 23 GPa) surface layers with excellent adhesion to the substrate. A 10–20 µm thick surface compound layer (1200HV) and 200–300 µm inner diffusion layer with very good mechanical and corrosion-resistant properties can also be formed on steel substrates in only 3–5 min by use of the PEN/PEC saturation techniques. Details are given of the basic operational characteristics of the various techniques, and the physical, mechanical and tribological characteristics of coatings produced by plasma electrolytic treatments are presented. © 1999 Elsevier Science S.A. All rights reserved.

Keywords: Arc plasma; Carburizing; Electrolysis; Nitriding; Oxidation; Spark discharge

1. Introduction

This paper reviews some relatively new electrochemical treatment processes categorised under the generic title of ‘Plasma Electrolysis’. Particular emphasis is drawn to their potential for future use in surface modification and coating. Despite some differences in the materials that can be treated, processing parameters and results obtained, these techniques should be considered as a distinct group of surface engineering processes due to the presence of, in each, the two following characteristic phenomena. Firstly, the electrolysis of a liquid environment by application of different electrical potentials between the workpiece material and a counter-electrode. Secondly the production of an electrical discharge at, or in the vicinity of, the workpiece surface.

Although the discharge phenomena associated with electrolysis were discovered more than a century ago by Sluginov [1] and were studied in detail in the 1930s by Günterschultze and Betz [2], their practical benefits were first exploited only in the 1960s, when McNiell and Gruss used a spark discharge to deposit cadmium niobate onto a cadmium anode in an Nb-containing electrolyte [3,4]. During the 1970s oxide deposition on an aluminium anode under an arc discharge condition was also developed and studied by Markov and coworkers [5,6]. Later this technique was improved and termed (apparently misleadingly) ‘micro-arc oxidation’ [7]. In the 1980s the possibilities of utilising surface discharges in oxide deposition onto various metals were studied in more detail in Russia by Snezhko and coworkers [8–13], Markov and coworkers [14–16], Fyedorov et al. [17], Gordienko and coworkers [18–20] and in Germany by Kurze and coworkers [21–24], where early industrial applications were introduced [25–29]. Researchers in both the USA and China have also become involved in

* Corresponding author. Tel.: +44-1482-465073; fax: +44-1482-466477.

E-mail address: a.matthews@eng.hull.ac.uk (A. Matthews)

this field [30–33]. Owing to the relatively sparse information on process phenomenology and, sometimes, a lack of understanding, different (and not always physically correct) terminology has been used in much of the above studies for what is, essentially, the same technique: ‘micro-plasma oxidation’, ‘anode spark electrolysis’, ‘plasma electrolytic anode treatment’, ‘Anodischen Oxidation unter Funkenentladung’ (anode oxidation under spark discharge), being typical examples of descriptions common to ‘plasma electrolytic oxidation’ (PEO).

Parallel to these developments, the heating effects of surface discharges in liquid electrolytes were observed by Lazarenko and coworkers [34–36] and utilised for metal heat treatment purposes. This technique was termed ‘heating in electrolytic plasma’. Further, Duradzy and coworkers studied thermal diffusion effects during plasma electrolytic heating [37–39], where the phenomenon of electrolyte elemental diffusion into the surface of the electrode was also noticed. During the 1980s these effects were used to develop a set of processes directed towards the surface saturation of bulk materials with various alloying elements [39,40]; thus new possibilities for the industrial application of the technique termed ‘plasma electrolytic saturation’ (PES) emerged. However, further development of the plasma electrolytic processes to fulfil their potential in a broader range of surface engineering applications requires a better understanding of the physical and chemical background of the plasma phenomena occurring on the electrode during electrolysis. In order to emphasise the common principles of the above plasma electrolytic processes the generic term plasma electrolytic deposition (PED) is used in this paper to include the sets of techniques that normally go under the headings of PEO and PES.

2. Physical and chemical fundamentals of plasma electrolysis

2.1. Phenomenology

It is well known that the electrolysis of aqueous solutions is accompanied by a number of electrode processes (Fig. 1). In particular, the liberation of gaseous oxygen and/or metal oxidation occurs on the anodic surface. Depending on the electrolyte chemical activity in respect to the metal, the oxidation process can lead either to surface dissolution or to oxide film formation. Liberation of gaseous hydrogen and/or cation reduction can also occur on the cathodic surface. When a ‘conventional’ electrolytic process is studied (e.g. electroplating, electrochemical machining, anodising, etc.), the electrode processes are usually considered in the framework of a simplified model, where the electrode–electrolyte interface can be represented by a

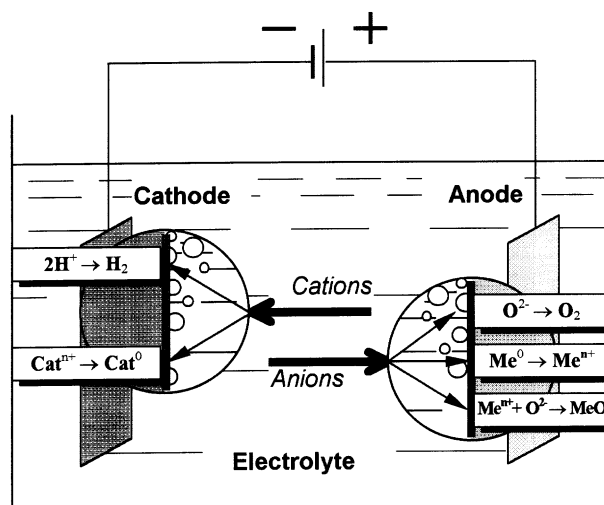


Fig. 1. Electrode processes in electrolysis of aqueous solutions.

two-phase system (i.e. metal–electrolyte or oxide–electrolyte couple) with a single phase boundary consisting of a double-charged layer. Concurrent by-product processes (such as gas liberation) are either neglected or taken into account using special correction factors, e.g. ‘current yield’ or ‘electrode shielding’ coefficients. However, as will be shown in the following, such a simplification is not always justifiable, since, under certain conditions, the results obtained from the treatment are influenced considerably by the processes that occur in the gaseous environment surrounding the electrode and/or in its surface layers.

2.1.1. Current–voltage characteristics

The above-mentioned processes affect the characteristic current–voltage profile of the electrochemical system (Fig. 2). A ‘type-a’ current–voltage plot represents a metal–electrolyte system with underlying gas liberation on either the anode or cathode surface; ‘type-b’ represents a system where oxide film formation occurs [39,41]. At relatively low voltages the kinetics of the electrode processes for both systems conform to Faraday’s laws and the current–voltage characteristics of the cell vary according to Ohm’s law. Thus, an increase in voltage leads to a proportional rise in the current (region ‘0– U_1 ’ in the type-a system and ‘0– U_4 ’ in the type-b system). However, beyond a certain critical voltage, the behaviour of a particular system may change significantly.

For a type-a system in the region U_1 – U_2 , a potential rise leads to current oscillation accompanied by luminescence. The current rise is limited by a partial shielding action of gaseous reaction products (O_2 or H_2) over the electrode surface. In areas where the electrode remains in contact with the liquid, however, the current density continues to rise, causing local boiling (ebullition) of the electrolyte adjacent to the electrode. Upon pro-

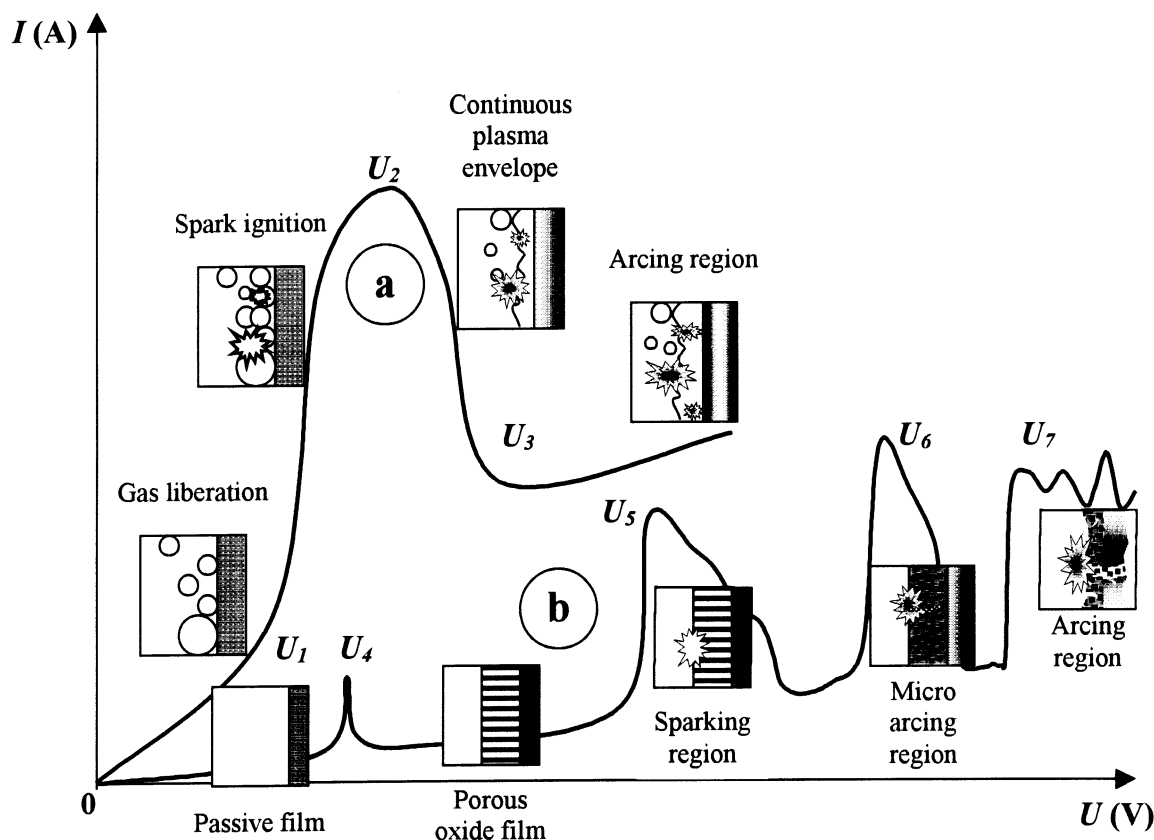


Fig. 2. Two kinds of current–voltage diagram for the processes of plasma electrolysis: discharge phenomena are developed (a) in the near-electrode area and (b) in the dielectric film on the electrode surface.

gression to point U_2 the electrode is enshrouded by a continuous gaseous vapour plasma envelope of low electrical conductivity. Almost all of the voltage across the cell is now dropped in this thin, near-electrode region. The electric field strength E within this region therefore reaches a value between 10^6 and 10^8 V/m, which is sufficient for initiation of ionisation processes in the vapour envelope. The ionisation phenomena appear initially as a rapid sparking in scattered gaseous bubbles and then transform into a uniform glow distributed throughout the vapour plasma envelope. Due to the hydrodynamic stabilisation of the vapour envelope in the region U_2 – U_3 , the current drops and, beyond point U_3 , the glow discharge transforms into intensive arcing accompanied by a characteristic low-frequency acoustic emission.

The behaviour of type-*b* systems is more complicated. Firstly, the passive film previously formed begins to dissolve at point U_4 , which, in practice, corresponds to the corrosion potential of the material. Then, in the region of repassivation U_4 – U_5 a porous oxide film grows, across which most of the voltage drop now occurs. At point U_5 , the electric field strength in the oxide film reaches a critical value beyond which the film is broken through due to impact or tunnelling ionisation [42,43]. In this case, small luminescent sparks are observed to

move rapidly across the surface of the oxide film, facilitating its continued growth. At point U_6 , the mechanism of impact ionisation is supported by the onset of thermal ionisation processes and slower, larger arc-discharges arise. In the region U_6 – U_7 thermal ionisation is partially blocked by negative charge build-up in the bulk of the thickening oxide film, resulting in discharge-decay shorting of the substrate. This effect determines the relatively low power and duration of the resultant arc discharges, i.e. micro-discharges, which are (somewhat misleadingly) termed ‘micro arcs’ [7]. Owing to this ‘micro-arcing’, the film is gradually fused and alloyed with elements contained in the electrolyte. Above the point U_7 , the arc micro-discharges occurring throughout the film penetrate through to the substrate and (since negative charge blocking effects can no longer occur) transform into powerful, arcs, which may cause destructive effects such as thermal cracking of the film [41].

In practice, a number of the above electrode processes may occur concurrently over adjacent areas of the electrode surface. The simple two-phase electrode–electrolyte model normally encountered in conventional electrolysis must therefore be replaced by a more complex four-phase system (metal–dielectric–gas–electrolyte) with a number of possible phase boundaries —

particularly when electrochemical systems running above the critical voltages of U_1 and U_5 are considered. Two phases of low conductivity are formed (i.e. dielectric and gas), where the main voltage drop is concentrated. Since the resistance of these phases varies continuously, it is very difficult to discern in what phase the ionisation phenomena are initiated [23]. Thus, the division of electrochemical systems into the two types is not distinct.

2.1.2. Discharge parameters

The concurrent combination of electrode processes in practical electrochemical systems, as well as the uniformity of electric field strength and electrolysis parameters, contribute to the wide diversity of discharge characteristics observed during plasma electrolysis. Owing to this, the observed plasma phenomena are related by researchers to the different discharge types, such as 'glow' [39,44], 'corona' [39,45], 'spark' [32,41], or 'arc-plasma' [46,47] discharges. Some of the principal characteristics of discharges in oxide films grown on aluminium are summarised in Table 1 [10,24,32].

Estimations of the discharge temperature also vary widely, from 800–3000 K [32] to 3000–6000 K [7,21,48] and even 10 000–20 000 K [48]. These differences may be attributed to the complex structure of the discharge channel, in which a hot core (of 6800–9500 K) and 'cold' circumferential area (of 1600–2000 K) have been identified by spectral studies [49]. The diameter of the discharge channel and the thickness of heat-affected zone are estimated to be 1–10 μm and 5–50 μm respectively [10,41,49].

2.2. Critical voltage points

For practical systems the current–voltage regions corresponding to the conditions of plasma electrolysis can be determined by the critical voltage points U_i indicated in Fig. 2. The critical values of U_i can often be quite accurately estimated on the basis of theoretical or empirical expressions. Thus, U_1 can be assessed against the critical field strength E_{c1} for breakdown

across a gaseous envelope, as follows from the theory of impact ionisation [50]:

$$E_{c1} = bp \ln \frac{\alpha}{ap}. \quad (1)$$

Here a and b are constants, p (Pa) is the vapour pressure and α is the impact ionisation coefficient of the vapour species.

From Eq. (1) the breakdown voltage U_1 of a vapour bubble in water can be estimated to be ~ 40 V, which lies close to the experimentally observed spark ignition voltage (which is usually 40 to 80 V) in both cathodic and anodic processes [32,51].

Region U_2 – U_3 can be estimated from the critical value of Joule heat density W_c for conversion from vapour bubbles to continuous film boiling:

$$jU_{(2-3)} = W_c. \quad (2)$$

Here j is the current density. Assuming that W_c for aqueous electrolytes is close to the critical density of heat flow for a water boiling process (i.e. $\sim 8 \times 10^5 \text{ W/m}^2$) [52] and that j can vary in the range 4–10 kA/m^2 , it is easy to estimate $U_{(2-3)}$ as being between 80 and 200 V, which is also in accordance with experimental data [51].

The breakdown voltage U_5 can be calculated using a modified equation of Günterschultze which has been confirmed experimentally [2,41–43]:

$$U_5 \cong \frac{E}{\alpha} \ln \frac{z}{a\eta C^b}. \quad (3)$$

Here a and b are constants, C is the electrolyte concentration, z is the elemental charge, and η is the electron current fraction of the total current passing through the system.

Values for U_6 and U_7 can be estimated from the theory of thermal ionisation of solids [50] taking into account the effective thickness ($2h^*$ for U_6) or the total thickness ($2h$ for U_7) of the dielectric film. The critical field strength E_{c2} for the development of ionisation processes in solids

Table 1
Surface discharge parameters for PEO of aluminium

Discharge parameter	Electrolyte			
	8.2% Na ₂ SiO ₃	8% NaAlO ₂	96% H ₂ SO ₄	NaF–Na ₂ CO ₃
Arc/spark density ($\times 10^{10} \text{ m}^{-2}$)	2	1–3	0.1	0.1
Discharge frequency (kHz)	3	0.5–2	10	–
Arc/spark duration ($\times 10^{-4} \text{ s}$)	2	0.1–1	2	0.1–0.2
Charge density ($\times 10^4 \text{ C m}^{-2}$)	3	0.2–2	0.02	–
Current density ($\times 10^8 \text{ A m}^{-2}$)	3	0.4–4	0.1	>0.1

is described by the expression [50]

$$E_{c2} = \frac{\beta_0 e^{(\beta_0 h \beta_0) C} \sqrt{\frac{2k}{a\gamma_{a0}}}}{hch\beta_0} \quad (4)$$

Here β_0 and C are tabulated parameters; k is a heat conductivity coefficient; a is the coefficient in the equation $\gamma_a = \gamma_{a0} e^{a(T-T_0)}$, where γ_{a0} is the active (electric) conductivity of a dielectric at temperature T_0 . Experimental estimations [49] show good agreement with Eq. (4), but only for films thicker than 30 μm .

2.3. Plasma-enhanced physico-chemical processes

Plasma phenomena considerably change the basic electrode processes because of both the enhancement of by-product physical and chemical processes and the instigation of new processes on the electrode surface (Fig. 3). Thus, thermal and diffusion processes, new plasma chemical reactions and macro-particle transportation (i.e. cataphoretic effects) become possible during electrolysis. These processes are utilised in the

various applications of plasma electrolysis, which include plasma-enhanced heat treatment and melting [39], welding [53], cleaning [54], etching and polishing [39,55], diffusion depletion [55] and deposition (i.e. PED) [7,39,41,56–59]. Among these plasma electrolytic techniques the PED group [which comprises the methods of PEO [7,39,41,59] and PES — including plasma electrolytic carburising (PEC) [56], plasma electrolytic nitriding (PEN) [57], plasma electrolytic boriding (PEB) [58], etc.] show excellent promise as cost-effective techniques for forming surface layers of high tribological, corrosion and thermal barrier performance. It follows from Fig. 3 that the layers are formed as a result of the modification of the basic electrode processes, principally by plasma-enhanced chemical reactions and diffusion processes on the electrode surfaces. This is primarily anode oxidation, in the case of PEO, and solution electrolysis and cation reduction, in the case of PES. The role of other plasma-enhanced physical-chemical processes in surface layer formation is less obvious; however, they are often interdependent with the chemical and diffusion processes and hence also deserve more detailed consideration.

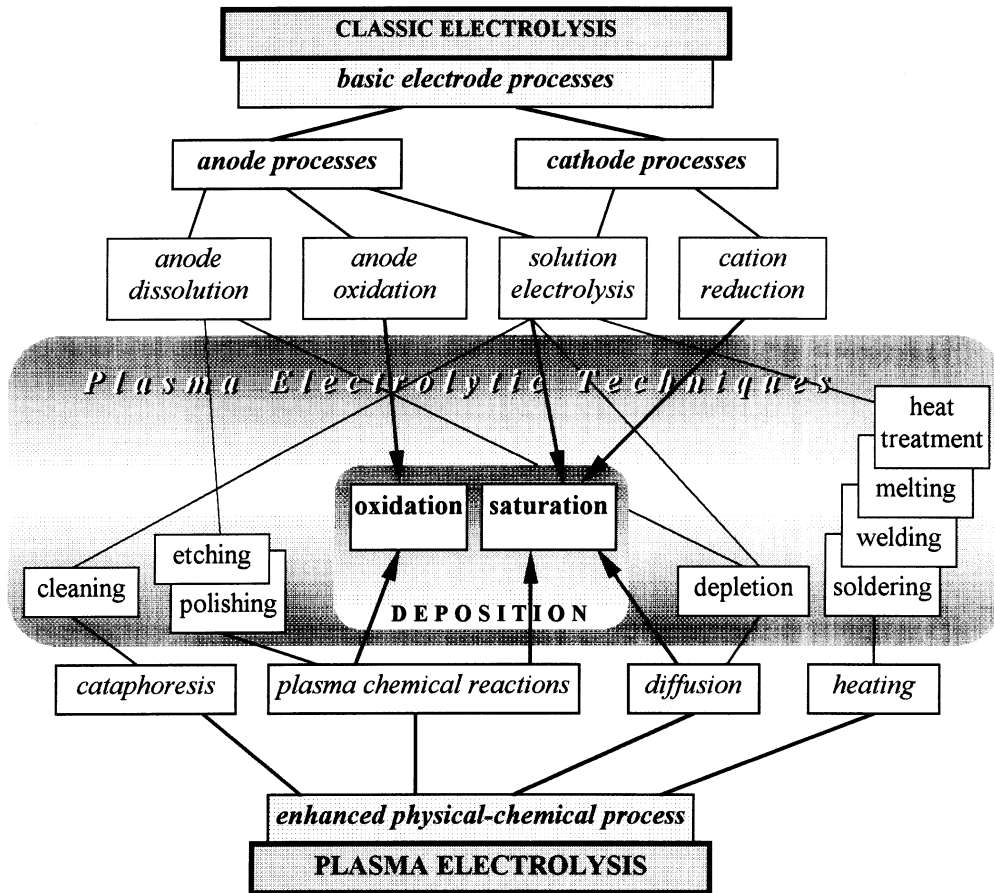


Fig. 3. Relationship between the principal physical-chemical processes occurring in plasma electrolysis and the basic electrode processes of classic electrolysis in the techniques of plasma electrolytic processing.

2.3.1. Heat evolution in plasma electrolysis

The heat balance at the electrode surface in plasma electrolysis is defined by the incident heat Q liberated in the near-electrode region and by the heat absorption of the metal substrate and electrolyte. Two components make up the net heat flux Q that arises from the chemical reactions taking place and the ohmic heating effect of the current flow I carried through the surface [60]; thus

$$Q = \Sigma \Delta H_i + \Delta UI, \quad (5)$$

where $\Sigma \Delta H_i$ describes the sum of the enthalpies of the chemical reactions occurring on and in the vicinity of the electrode surface, and ΔU describes the voltage drop across the region adjacent to the electrode. Among these components, ohmic heat dominates in the near-electrode area, because the voltage drop ΔU is concentrated in the phases of low conductivity, such as the vapour envelope and/or (particularly in the case of PEO) the growing oxide film. The power generated from ohmic heating at the electrode surface can be very significant and is estimated to be typically 0.1 to 1 MW/m². The power generated from exothermic electrochemical process, combined with that of plasma thermochemical ion momentum-transfer reactions on the electrode surface is usually less than one-third of that generated from ohmic heating. These sources of heating are balanced by the heat absorption of both the electrode–substrate and the electrolyte [52]:

$$Q + \alpha(T_s - T_e) = -\lambda_s \frac{\partial T}{\partial x}. \quad (6)$$

Here T_s and T_e are the temperatures of the substrate and the electrolyte respectively; λ_s is the substrate heat conduction coefficient and α is the heat-transfer coefficient at the electrode–electrolyte interface. The heat-transfer coefficient can vary over a wide range, depending on the conditions of heat exchange at the electrode–electrolyte interface [52]. By analogy with the water boiling process, the different conditions corresponding to bubble formation and film boiling can be discerned in plasma electrolysis to produce, respectively, a discontinuous or continuous gaseous envelope [61]. The heat exchange diagram presented in Fig. 4 shows that the incident heat flux is the primary factor defining the conditions of heat exchange on the electrode surface. However, intensive gas liberation caused by electrode oxidation/reduction processes, as well as the hydrodynamic action of spark and arc discharges, introduces certain peculiarities to the diagram. Though gas liberation may lead to an extension of the region of continuous vapour envelope stabilisation to lower heat flows, the establishment of discharge conditions can, conversely, enhance steady-state bubble boiling.

Two factors facilitate the production of localised discharges in the area adjacent to the electrode; these

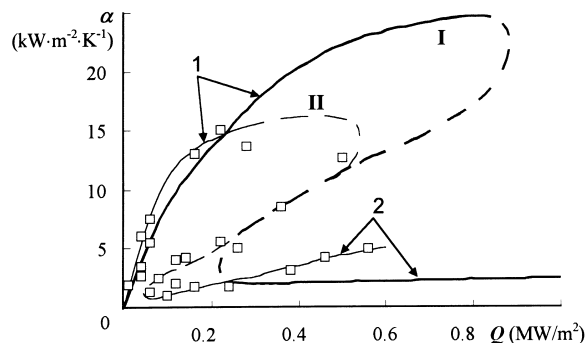


Fig. 4. Heat exchange diagram for the processes of (I) water boiling [52] and (II) plasma electrolysis. Plots 1 and 2 correspond to the conditions of bubble boiling and vapour film stabilisation respectively. The squares are derived from PEO experimental data [61].

are (i) the non-uniform distribution of the electric field in the vicinity of the electrode and (ii) the presence of a dielectric film on its surface. More intensive arcing is, therefore, usually observed on sharp edges of the work-piece in both PEO and PES processes. Furthermore, the formation of a passivating (oxide) film in the PEO process promotes arcing over the whole surface. Bubble boiling conditions are, therefore, particularly common for PEO processes [61]. Under such conditions the heat-transfer coefficient generally rises in proportion to the increasing applied heat flux, and therefore T_s either does not rise, or rises only slowly, to no more than 100–180°C (Fig. 5).

Conversely, if a dielectric film cannot be formed on the electrode surface, then the continuous vapour envelope conditions are quickly realised, and α increases only slightly with the applied heat flux (region 2 in Fig. 4). Under these conditions high-rate heating of the electrode surface is possible. At low values of α , the near-surface temperature can reach 900 to 1200°C in only 1 to 3 min, over a wide range of working potentials (Fig. 6) [51,62]. Here T_s becomes a linear function of the applied voltage, which, according to Eq. (5), implies

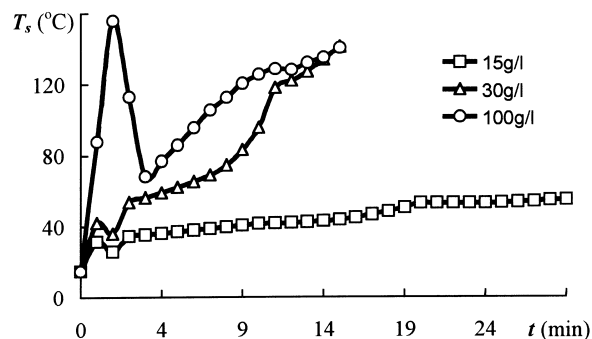


Fig. 5. Temperature of Al substrate versus time of PEO processing in a silicate-containing aqueous electrolyte. Net heat flux Q at electrolyte concentration of 15 g/l, 30 g/l and 100 g/l varied in the ranges 0.1–0.05 MW/m², 0.2–0.1 MW/m² and 0.5–0.3 MW/m² respectively [61].

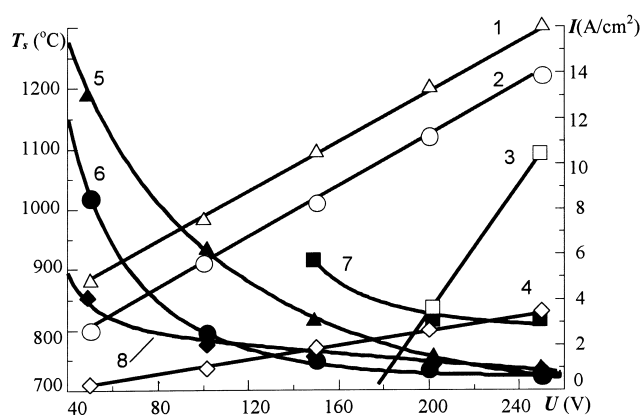


Fig. 6. Potential–temperature (1–4, i.e. filled) and potential–current (5–8, i.e. unfilled) characteristics of PES processes: 1,5 – boriding [62]; 2,6 – carburizing [62]; 3,7 – carbonitriding [51]; 4,8 – nitriding [62].

a negligible contribution from the chemical heating components to the overall heat flux at the electrode surface. Nevertheless, modification of the near-surface composition can still occur, primarily through rapid inward diffusion processes initiated by a high (local) surface temperature and enhanced by high current density/low energy ion implantation (from the ionised gas in the vapour envelope) under the applied electrical field of, typically, several hundred volts.

2.3.2. Diffusion processes

The difference in chemical composition between the heated surface of the metal electrode and the vapour envelope is what drives the diffusion processes in PED techniques. Both diffusion of elements inward to the metal substrate (i.e. saturation) and outward to the surface (i.e. depletion) are observed. Surface saturation is possible both in anodic and cathodic processes. Depending on the electrolyte, compositional saturation by nonmetal elements, such as O, C, N, B (and combinations of these), or by carbide-forming transition metal species, such as W, Mo, V, etc., is possible [39].

The saturation of anodic surfaces with nonmetallic elements is usually effected using aqueous solutions of simple inorganic acids, suitable salts containing the

desired elements and certain organic compounds (Table 2). The diffusant species are chosen such that they become negatively ionised in the electrolyte, and thus are drawn into the vapour envelope under the influence of the applied electric field and accelerate across the voltage drop to bombard the electrode surface. Interstitial and grain-boundary diffusion mechanisms are prevalent in the growth of compounds in the anodic layer. The limiting diffusant content in the electrode surface is determined by its concentration in the adjacent vapour envelope. Furthermore, compound formation on the anode is often also accompanied by an oxidation process; therefore, an oxide layer is often present on top of the (for example) carbide, nitride or boride layer. To avoid surface oxidation, cathodic polarisation techniques can be used. However, the electrolytes used for cathodic formation of compound layers are generally more complex and may also require the use of toxic and/or combustible organic substances to be effective.

Metallic diffusion into an electrode surface can be effected using solutions of heteropoly acids. The diffusant is adsorbed onto the electrode surface, where a polymeric layer is formed. Further diffusion of the metal elements occurs by a diffusion displacement mechanism. The maximum diffusant content in the electrode is defined by its concentration in the adsorbed polymeric layer. To raise the diffusant concentration in the layer, the electrolyte concentration can be increased and/or acids with longer polymeric chains can be used. However, such measures may lead to an increasing propensity for the electrolyte to polymerise. As with nonmetallic diffusion, the polymer layer adsorbed onto the surface needs to be removed after treatment for reasons of both poor physical/mechanical performance and aesthetic appearance.

Despite the disadvantages mentioned above, the extraordinarily high rates of diffusion available from such methods are a notable feature of the PES technique. In comparison with conventional thermally activated saturation processes (e.g. gas carburising or pack metallising) the effective diffusion coefficient in plasma

Table 2
Electrolyte compositions for PES processes

Process	Purpose	Electrolyte composition
Nitriding	Improvement of surface hardness, wear and corrosion resistance, fatigue strength	NaNO ₃ , 45%
Carburizing	Improvement of surface hardness, wear resistance and fatigue strength	C ₃ H ₅ (OH) ₃ , 15%; Na ₂ CO ₃ , 5%
Boriding	Improvement of surface hardness, heat corrosion and wear resistance	Na ₂ B ₄ O ₇ , 3%; NaOH, 45%
Carbonitriding	Improvement of surface hardness and wear resistance	C ₃ H ₅ (OH) ₃ , 15%; Na ₂ NO ₂ , 45%
Nitroboriding	Improvement of surface hardness and corrosion resistance	Na ₂ B ₄ O ₇ , 3%; NaNO ₂ , 45%
Carbonboriding	Improvement of surface hardness and wear resistance	C ₃ H ₅ (OH) ₃ , 15%; Na ₂ B ₄ O ₇ , 3%; NaOH, 10%
Carbonitriding + boriding	Improvement of surface hardness and corrosion resistance	C ₃ H ₅ (OH) ₃ , 15%; Na ₂ B ₄ O ₇ , 3% NaNO ₂ , 45%

electrolysis is increased by 200 to 250% for nonmetal elements and by 30 to 50% for metal species [39]. These effects may be influenced by the following factors:

1. reduction of activation energy for the diffusion process in the electric field;
2. surface activation and adsorption improvement of diffusants due to the influence of an electrical discharge;
3. increased bulk diffusion due to the development of lattice defects (such as vacancies and dislocations), as a result of the action of the discharge.

2.3.3. Plasma chemical reactions

Another feature of plasma electrolysis is the formation of specific surface structures such as metastable high temperature phases, nonequilibrium solid solutions, complex mixed-compounds, glassy phases, etc. These substances are formed as a result of plasma thermochemical reactions at the electrode surface. Depending on the conditions realised in the near-electrode region, the reactions may occur either in the discharges developed in the vapour envelope or directly in the surface layer. Accordingly, both vapour-phase and solid-state plasma thermo-chemical reactions are found. Owing to the flexible vapour–liquid interface the reactions of the first type run at relatively low instantaneous pressures and temperatures ($p \approx 0.15$ to 0.2 GPa, $T \approx 1000$ to 1500°C). At higher values ($p \approx 10^2$ GPa and $T \approx 2 \times 10^4^\circ\text{C}$) the second type of reaction is more commonly found.

In accordance with the dynamics of the discharge phenomena the chemical interactions of plasma electrolysis occur in two steps: ionisation and condensation [63]. In the first step, impact or thermal ionisation occurs in the discharge area. Processes occurring here consist primarily of compound dissociation. These processes progress rapidly with a considerable exothermic effect and volume expansion. Owing to this, the plasma in the discharge channel reaches high temperatures and pressures in a time period of less than 10^{-6} s. The electric field in the discharge channel separates the charged particles in the plasma. Some of them (for example positive ions) are released into the electrolyte and the rest (for example negative ions) participate in processes on the electrode surface.

During the second step, the temperature rapidly drops and the components of the plasma form products that are condensed within the discharge channel. Since the cooling rate reaches 10^8 K/s, unique high temperature phases, supersaturated solid solutions and nonequilibrium compounds can be fixed on the surface at near ambient temperature. Thus, the fabrication of α - and γ - Al_2O_3 [64], TiO_2 (anatase and rutile) [65], α - SiO_2 [41], δ - Nb_2O_5 [66,67], CdNb_2O_6 [21], Al_2TiO_5 [65], BaTiO_3 [65], NaNbO_3 [66], $3\text{Al}_2\text{O}_3 \cdot 2\text{SiO}_2$ (mullite) [17,64] and several other compounds on the electrode surfaces have previously been reported.

Phase composition is the principal factor that determines the real mechanical or tribological performance of the surface layer. Forecasting phase composition in the treated layer is, therefore, an important applied problem in PED. The exact solution is quite difficult to determine, particularly considering the difficulties of accurately defining the complex kinetic parameters describing all the reactions taking place in the discharge region. A qualitative approach to solving this problem has been developed [67], in which the probability of phase formation in the surface layer is estimated using phase equilibrium diagrams for the corresponding system. A more fruitful approach allowing for a quantitative (within 20% error) estimation of the layer phase composition was developed in Refs. [27,68], especially for PEO of aluminium. Its execution lies in the step-by-step thermodynamic calculation of equilibrium products for the reactions occurring in the ionisation and condensation stages of the discharge process. The calculations are based on the principle of maximisation of entropy for the hetero-phase multi-component system, which is a model of the discharge channel. Within the framework of such an approach it is possible to study the effect of characteristics of the discharges employed and the effects of channel composition, its geometry (diameter and aspect ratio) and thermodynamic state (p and T). This capability can be useful for the designation and optimisation of treatment regimes for plasma electrolysis.

2.3.4. Cataphoretic effects

Cataphoretic effects, i.e. macroparticles transferring both towards and away from the electrode surface, are possible in the strong electric fields realised in plasma electrolysis. The transfer is promoted by hydration and charging of macroparticles, as well as hydrodynamic effects caused by surface discharge heating and convection. Though outward transfer can be used to clean the surface [54] and remove coatings and films deposited by other methods [69], transfer towards the surface is also widely utilised in enhancing coating deposition.

The macroparticle size and the energy density in plasma electrolytic processes are two principal factors that govern cataphoretic processes (and thus surface structure) in coating deposition. Firstly, the cataphoretic deposition of sub-macroparticles (i.e. micelles of 10 to 100 nm in size) from colloidal solutions and the deposition of macroparticles (i.e. powders of 1 to 20 μm in size) from suspensions in solution can be distinguished. Colloidal solutions of inorganic polymers, such as silicates, aluminates, polyphosphates, tungstates, molybdates, etc., and slurries of powders of oxides, nitrides, carbides, borides, etc., can all be used to provide enhanced coating modifications.

Secondly, the electrical regimes in plasma electrolysis can be classified into three distinct groups:

1. regimes that promote macroparticle sublimation in the discharge surrounding the electrode;
2. regimes that encourage sintering of macroparticles on the electrode surface;
3. regimes that generate complete fusion of macroparticles within the growing film.

Although the particular current mode to be used and the values of electrical parameters of the process depend on the particular electrolyte–electrode combination, the broad classifications outlined above allow a prognosis on the possible structure of deposits; i.e. (i) pseudo-diffused, (ii) agglomerated or (iii) dense-fused [66].

3. PED technology

3.1. Equipment

A typical treatment unit for PED processing consists of an electrolyser and a high power electrical source (Fig. 7). The electrolyser is usually a water-cooled bath made of stainless steel, which also serves as the counter-electrode. It is placed on a dielectric base and confined in a grounded steel frame, which has an insulated current supply and a window to observe the process in operation. The electrolyser incorporates electrolyte mixing, recycling, and gas exhausting arrangements, as well as electrical interlocks. The earthed frame (with dielectric base), interlocked door and ventilated exhaust are designed to provide safety for the operating personnel.

Various types of power source can be used to bring about plasma electrolysis [8,41,70–72]. According to the applied electrical regime they can be classified into the following groups.

3.1.1. DC sources

These are normally based on a bridge circuit and allow the application of galvanostatic or potentiostatic

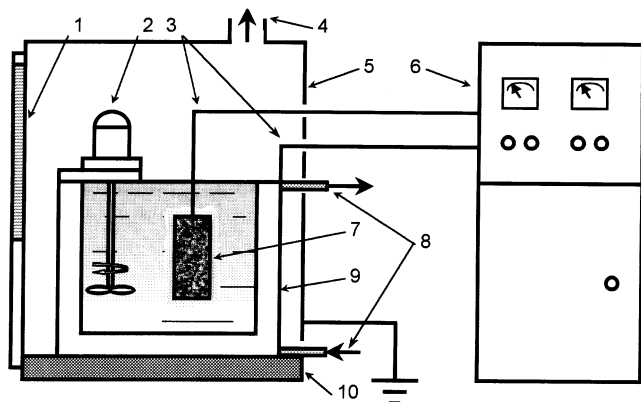


Fig. 7. Typical arrangement of the equipment used for PED treatment: (1) window, (2) mixer, (3) connecting wires, (4) exhaust/ventilation system, (5) grounded case, (6) power supply unit, (7) workpiece, (8) cooling system, (9) bath, (10) insulating plate.

regimes of direct current. However, the possibility for controlling the PED process is limited, because of difficulties in regulating the surface discharge characteristics. For such reasons DC power sources are used only for simple-shape components and thin coatings.

3.1.2. Pulsed DC sources

The application of pulsed DC allows for controlled interruption of the process and thus the arc duration; the pulse form can also be changed. Both of these features allow the heat conditions during treatment to be controlled, and thus the coating composition and structure changed. However, a pulsed current can give rise to an additional polarisation of the electrode surface caused by the creation of a charged double layer. In this case higher voltages (up to 1000 V) may be needed to achieve the desired current density. Pulsed DC regimes find wide application in PES, where a relatively low voltage (typically less than 450 V) is required. For example, a 10 kW silicon-controlled rectifier allowing pulsed DC output at 0 to 450 V is reported to have been applied in a plasma electrolytic carbonitriding (PEC/N) process [51].

3.1.3. Unbalanced AC sources

Additional polarisation of the electrode can be avoided by using AC sources, while the possibility of improved process control by means of arc interruption is retained. Furthermore, the application of unbalanced AC, i.e. an alternating current with different amplitudes to the positive and negative components, makes it possible to extend the controlled range of coating deposition. The simplest circuit of this type of power source is the controlled capacitor-based multiplier [73]. In this circuit, a set of high voltage capacitors redistributes electrical energy according to the total resistance of the cell in the positive and negative half-cycles. By varying the capacitance of the source in both half-cycles, the ratio of amplitudes of positive and negative current can be independently adjusted. Furthermore, when (for example) a UK three-phase mains voltage supply (415 V, 50 Hz) is applied, there is often no need for a powerful step-up transformer to obtain a higher voltage output. The beneficial combination of the added process control features, together with a simple and low cost source, has led to increased usage of such sources in laboratory-scale PEO processes. However, the limitations in the power (typically ≤ 10 kW) and current frequency (mains frequency only) are the principal disadvantages of these sources that restrict commercial upscaling.

3.1.4. Sources of heteropolar pulsed current

To supply higher power and/or a range of frequencies, heteropolar pulsed current sources can be used. These are based on thyristor- or transistor-reversible converters. Although thyristor-based circuits allow the pro-

duction of rectangular or truncated sinusoidal pulse shapes, transistors permit added flexibility in programmed pulse shapes, amplitudes and durations [72].

3.2. Deposition procedure

Owing to their underlying simplicity of operation, the PED processes compare favourably on cost with vacuum deposition and electroplating techniques. Sample pretreatment consists of cleaning and degreasing only. No additional operations, such as etching or surface activation, are required.

To deposit coatings, the samples are attached to the current supply of the unit and typically immersed in the bath at a depth of 30 to 50 mm beneath the electrolyte surface. A metal rod with a fluoroplastic jacket is typically used as a holder. After the electrolyte cooling, mixing and gas exhaust are activated, the working voltage can be applied to the electrolyser terminal and adjusted at the power supply in accordance with the selected treatment regime. The principal parameters of the process, such as the mean value of the current, the amplitudes of the anode and cathode voltages and the electrolyte temperature, are recorded. It should be noted that there are some peculiarities in the selection and monitoring of the process parameters that are distinct to either oxidation or nitride/carbide formation.

3.2.1. Process monitoring in PEO

Current density is the principal parameter to be controlled in routine PEO processing. Normally, to reach the required conditions for plasma electrolysis, the current density is set within the range 0.01 to 0.3 A/cm². According to Faraday's first law, this defines the coating growth rate. While the coating grows, the voltage increases, rapidly at first, then slowly, once steady-state plasma conditions have been established. The critical rate of voltage change corresponds to the establishment of a spark discharge on the electrode surface (U_5). This value has a strong dependence on the characteristics of metal–electrolyte combination and typically lies in the region 120 to 350 V. In the first step of the process sparking is observed as a uniform white light surrounding the electrode. As coating progresses this changes to a number of separate yellow sparks that move rapidly across the surface (U_6). Gradually, the spark density reduces; however, their power is increased. Finally, a few red arc spots moving slowly across the surface can be seen (U_7). From time to time powerful arcs can lead to current oscillations and coating damage. The process is therefore usually terminated immediately when a powerful arc is detected.

3.2.2. Process monitoring in PES

PES processing can be performed employing both anodic and cathodic polarisation of the workpiece. When selecting the workpiece polarity it should be taken

into account that anodic treatment is preferable if the presence of a thin outer oxide layer above the diffusion zone is not prohibitive. Cathodic treatment is often accompanied by hydrogen liberation and therefore calls for careful consideration of safety requirements.

In contrast to oxidation, voltage is the principal characteristic to be controlled in the PES treatment procedure. Process control consists of rapidly increasing the voltage in the first stage and maintaining the potentiostatic conditions in the second stage to stabilise the treatment temperature.

Early on in the first stage, the rapid voltage increase produces many bubbles at the electrode surface, due to intensive electrolysis of the solution and Joule heat liberation. The cell voltage–current characteristics conform to Ohm's law at this point. When the value U_1 (about 75 V) is reached, the vapour inside the bubble is broken-down and a spark discharge is observed. Increasing the applied voltage causes the spark intensity to increase. When the characteristic voltage U_3 is reached (close to 175 V), the surrounding electrode-bubble sparks transform to establish a continuous glow. The complete separation of the electrode from the electrolyte by a continuous vapour envelope at this point is reflected in a sharp reduction in current at the electrode surface. The conditions of PES treatment, where the sample temperature is a linear function of voltage, are now established. The current density is normally in the region of 0.5–1 A/cm² during treatment.

In the second stage, a certain voltage value is fixed to maintain the desired sample temperature. The plasma in the glow region contains activated ions of (for example) carbon and nitrogen, which are reactively deposited onto the surface and diffuse inwards under the influence of the high local temperature and concentration of active species. Under these conditions surface saturation can often be achieved in only 3 to 5 min and the process is then effectively complete.

For both processes, after the coating has been formed, the samples are simply cleaned (by flushing with water) and dried.

3.3. The effect of electrolyte composition

3.3.1. Electrolyte selection for PEO

The practical realisation of PED processing requires careful matching of the metal–electrolyte combination. For the PEO process this can be achieved on the basis of polarisation test data, which are commonly used to study metal passivation. The electrolytes that can be utilised in the production of oxide coatings on aluminium alloys are compared in Ref. [41]. Fig. 8 shows that the following six groups can be distinguished:

1. solutions of salts that provide fast dissolution of aluminium, e.g. NaCl, NaClO₃, NaOH, HCl, NaNO₃;

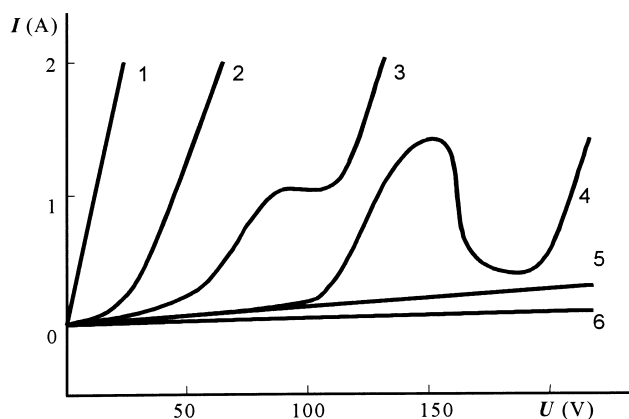


Fig. 8. The function $I=f(U)$ of various electrolytes tested for PEO treatment of aluminium. Anodic polarisation can lead to: (1) fast metal dissolution, (2) slow metal dissolution, (3) metal passivation in narrow voltage interval, (4) complex behaviour with a wide interval of passivation, (5) slight passivation and (6) strong passivation of the metal [41].

2. electrolytes providing slow metal dissolution, e.g. H_2SO_4 , $(\text{NH}_4)_2\text{S}_2\text{O}_8$, Na_2SO_4 ;
3. electrolytes providing metal passivation in a close range of voltages, e.g. sodium acetate or phosphoric acid;
4. fluoride electrolytes, which are characterised by complex behaviour, e.g. KF, NaF;
5. electrolytes promoting slight passivation of the metal;
6. electrolytes promoting strong metal passivation, e.g. boric acids and salts of carbonic and phosphoric acids, inorganic polymers (e.g. silicates, aluminates, tungstates, molybdates) and phosphates of alkaline metals (which can form polymer anions).

As can be seen in Fig. 8, the electrolytes from the groups (4)–(6) allow the sparking voltage to be easily reached and are the most beneficial for coating production by the PEO technique. These electrolytes are classified into four groups from the viewpoint of their contribution to the coating composition [73]:

- (a) solutions that incorporate only oxygen into the coating;
- (b) electrolytes containing anionic components that incorporate other elements into the coating;
- (c) electrolytes containing cationic components that incorporate other elements into the coating;
- (d) suspensions providing cataphoretic transport of macroparticles that contribute to the coating composition.

In the electrolytes of groups (b) and (c) the coating is formed both by substrate oxidation and by other electrolyte substances depositing on the substrate surface. This allows a wide range of modifications of the coating composition and properties and, therefore, these groups are considered as the most promising. Colloidal solutions of sodium or potassium silicate, as well as multi-component electrolytes based on silicates, are widely

used in PEO processes. Besides silicates, the solution can contain substances that increase the electrolyte conductivity [e.g. NaF (0.5 to 20 g/l), NaOH or KOH (1 to 50 g/l)] and/or provide the oxide layer with stabilising elements [e.g. $\text{Na}_2\text{B}_4\text{O}_7 \cdot 10\text{H}_2\text{O}$ (40 g/l), glycerine (10 g/l), Na_2CO_3 or K_2CO_3 (≤ 500 g/l)] and modifying components [e.g. NaAlO_2 (2 to 20 g/l), $\text{Na}_6\text{P}_6\text{O}_{18}$ (≤ 150 g/l)] [73–77]. For specific purposes fine powders of hard, high melting point materials and/or dry lubricants (for improved friction and wear), and/or colouring agents (for optical properties and decoration) can be introduced into the electrolytes, to integrate cataphoretic effects with the oxidation process.

3.3.2. Electrolyte selection for PES

Selection of the electrolyte is relatively simple for the PES process. As an example, for PEC/N the electrolyte is composed of C/N-containing organic compounds and 5–10% of an electrolyte in conductive solution, e.g. $\text{KCl} + \text{H}_2\text{O}$. In contrast to conventional pack- and liquid-based treatments using cyanide, various ecologically friendly organic compounds can be used to provide, by plasma thermal decomposition, desirable carbon/nitrogen ions and/or atoms for the treatment process [51]. Thus, formamide (HCONH_2), ethanolamine [$\text{H}_2\text{N}(\text{CH}_2)_2\text{OH}$] and carbamide [$\text{CO}(\text{NH}_2)_2$] are commonly used for nitriding, nitrocarburising and carburising respectively. Water content influences the electrical parameters; that is, less than 5% H_2O causes an increase in the critical voltages for plasma envelope stabilisation; more than 10% H_2O leads to a sharp increase in the slope of the voltage–temperature curve.

4. Surface composition and structure

4.1. Oxide coatings on aluminium alloys

Structural studies typically show three distinct regions in the coatings produced on Al-alloys by the PEO technique (Fig. 9). The porous outer region consists predominantly of low temperature and X-ray amorphous phases. A dense inner region is formed by high temperature modifications, whereas complex phases of the substrate alloying elements are observed in a thin, interfacial region below the dense layer. The relative sizes of the regions, their structure and composition are substantially influenced by substrate composition, electrolyte composition and treatment regime.

Comprehensive studies of these effects have been carried out for the treatment of Al-alloys in silicate solutions [78–80]. It has been observed that the application of alkali and dissolved-silicate/alkali solutions (e.g. 2–20 g/l Na_2SiO_3 and 2–4 g/l KOH) results in an extension of the inner dense layer, which consists mainly of γ - and α - Al_2O_3 phases (Fig. 9), with some complex

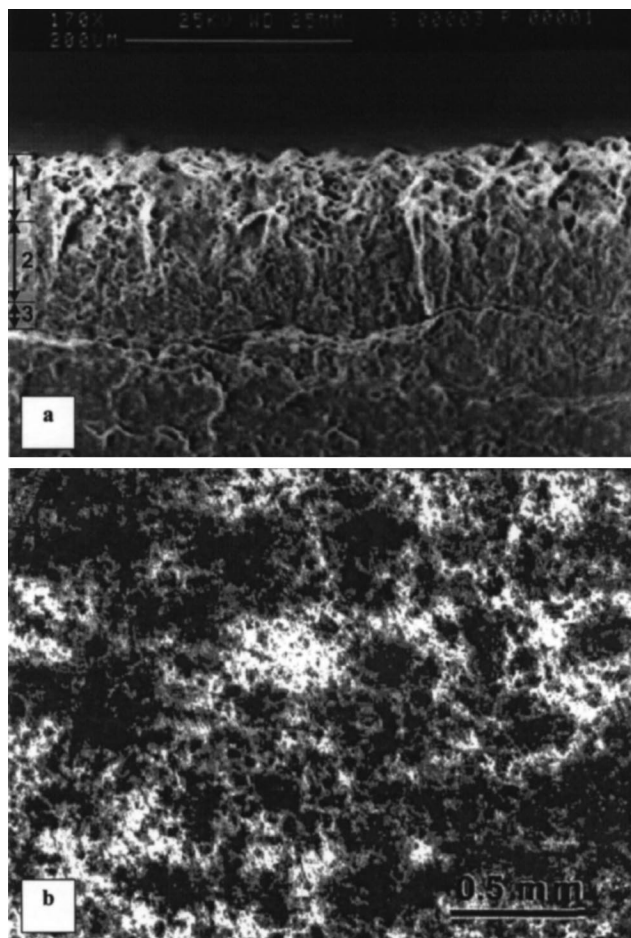


Fig. 9. Microphotographs of an oxide coating produced by the PEO technique on an aluminium alloy. (a) SEM image of the coating cross-section, where (1) is the porous (external) region, (2) is the dense intermediate (internal) region and (3) is a thin complex-phase (diffusion) region of the substrate alloy. (b) Optical image of the surface of the intermediate region after polishing to remove the porous outer layers showing the distribution of the high temperature alumina (bright) and aluminosilicate (dark) phases.

Al–Si–O phases also present. The relative proportion of the harder α phase is increased by raising the current density. The content of α -alumina can reach 60% for coatings formed on copper-containing aluminium substrates, whereas the γ -Al₂O₃ phase is predominantly formed on magnesium-containing aluminium alloys. Coatings based on the mullite phase are formed on silicon-containing substrate materials.

The effect of silicon is discussed in more detail in Ref. [79]. It is shown that raising the silicate concentration in the electrolyte leads to accelerated coating growth, due to the incorporation of Si into the coating structure and formation of complex Al–Si–O phases (Table 3). Thus a two-phase structured intermediate layer can be formed [Fig. 9(b)], where the phase ratios can be varied over a wide range.

The elemental distribution through the coating thickness when silicon is introduced into the alkali electrolyte is changed depending on the type of Si-containing particles [75]. Coatings formed in a 2 g/l alkali solution with no silicate additions exhibit a uniform distribution of Al through the thickness and specific substrate alloying elements (e.g. Cu and Mg) displaced towards the surface, according to their activity with oxygen (Fig. 10). The addition of sodium silicate at 15 g/l into the electrolyte leads to the penetration of 3 to 5 at.% silicon into the coating and a substantial reduction in Cu and Mg concentrations, which are in turn increased in the interfacial zone. Also the positions of maximum Cu and Mg content are shifted in to the substrate. When silica is introduced as a fine powder the Si content in the coating is raised considerably (up to 40 to 60% on the surface) but is distributed nonuniformly through the thickness. Accordingly, the profiles of Al and the other alloying elements are also changed.

When using dissolved silicate–alkali solutions the coating thickness uniformity depends in a rather complex manner on the electrolyte composition [80]. Uniform coatings can be produced at only certain balanced combinations of silicate and alkali. Increasing the silicate concentration leads to enhancement of the coating growth on the sample edges, where silica polycondensation processes are facilitated due to the more intensive arcing. Conversely, increasing alkalinity causes local dissolution of the oxide layer and pitting across the sample surface.

Oxide coatings produced in concentrated silicate solutions (50–300 g/l) are thicker and more uniform. They have, however, an extended outer layer, which can reach up to 90% of the total coating thickness. Such layers are predominantly X-ray amorphous and normally consist of 40 to 43% Si, 1 to 4% Al, 1 to 4% Na and 49 to 58% O [41]. As a rule, these silicate coatings possess a foam-like structure with high bulk porosity and rela-

Table 3
PEO regimes and some characteristics of oxide coatings produced on aluminium

Na ₂ SiO ₃ conc. (g/l)	Treatment time (min)	Current density (A/dm ²)	Coating thickness (μm)	Al–Si–O stoichiometry	Ratio of Al ₂ O ₃ to Al–Si–O
2	120	12	85	Al _{0.26} Si _{0.08} O _{0.06}	1.0
4	80	25	75	Al _{0.23} Si _{0.10} O _{0.67}	0.6
6	60	25	110	Al _{0.22} Si _{0.12} O _{0.65}	0.4
20	25	25	120	Al _{0.13} Si _{0.19} O _{0.68}	0.1

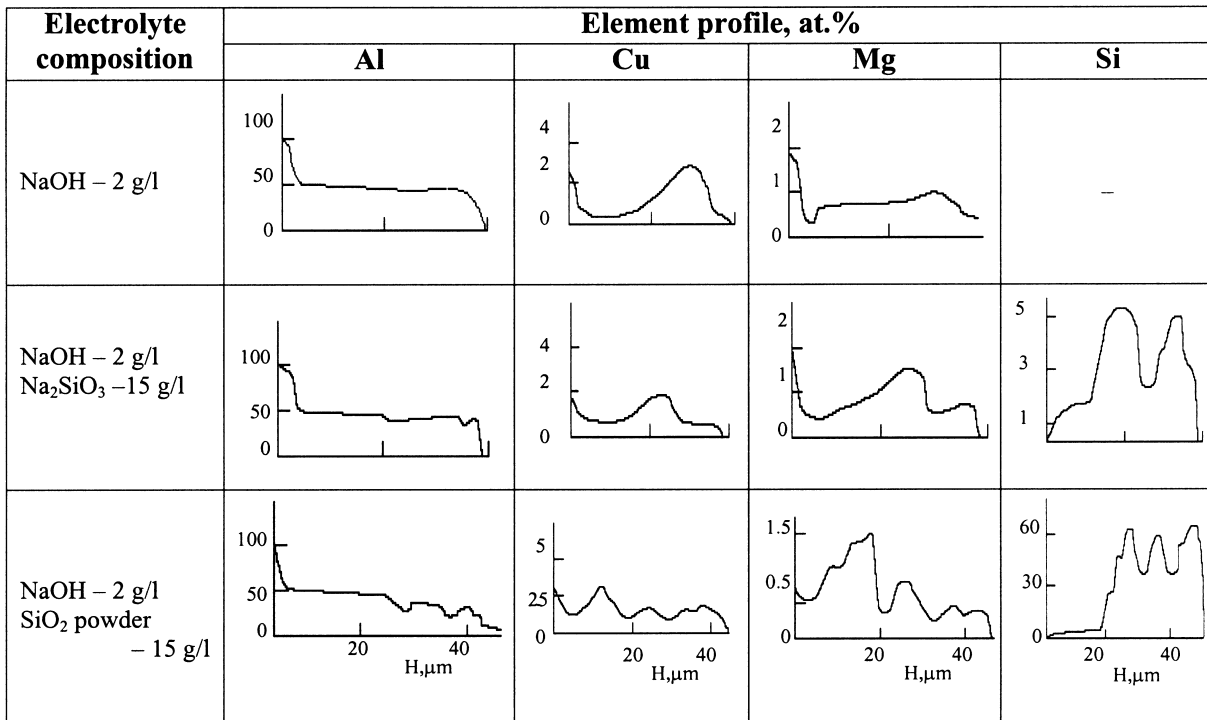


Fig. 10. Elemental distribution (atom percent) through oxide coatings produced by PEO treatment of Al 3.0Cu 1.5Mg 0.5Mn alloy in alkali and silicate-alkali solutions [75].

tively poor mechanical properties. The composition of these coatings can be changed only at the cost of additional substances being introduced into the electrolyte. Often, for these purposes, electrolytes containing fine powders of Al₂O₃, Fe₃O₄, TiO₂, MgO, Cr₂O₃ are used [27,28,41]. However, because of the high bulk porosity, the elemental distribution through such coatings is extremely non-uniform.

4.2. Nitride/carbide surface layers on steels

In a manner similar to conventional thermochemical diffusion treatments, the surface layers produced on steels by PEN/C consist of two regions. Below the surface, an inner diffusion zone of pearlite and retained austenite (with diffusing elements in solid solution) changes gradually to a non-etching outer ‘white’ layer, formed primarily by iron nitrides and carbides. The characteristics of these structural regions depend on the applied voltage (and thus temperature), treatment time and type of diffusing element. Fig. 11 shows the kinetic characteristics of PES of mild steel by carbon and nitrogen when applied either individually or concurrently [39]. It is clear that simultaneous diffusion of carbon and nitrogen provides a much faster saturation of the surface and a thicker treated layer. The electrode polarity slightly affects the saturation kinetics.

Cross-sectional micrographs of typical saturated surface layers produced by plasma electrolysis are presented

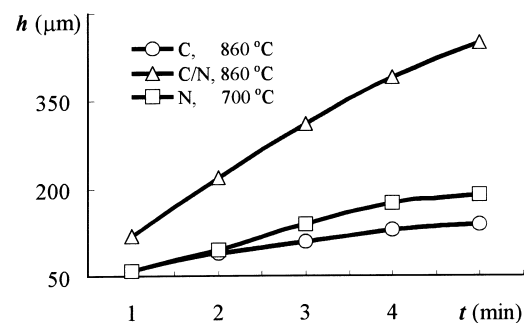


Fig. 11. Kinetics of coating growth under different conditions of the PES process [39].

in Fig. 12. The nitride coating consists typically of an outer white layer of the ϵ -Fe₂₋₃N phase bonded to an inner diffusion layer containing a mixture of nitrides and nitrogen-containing α -Fe_(N) phases, with a total thickness of 40–50 μ m [Fig. 12(a)]. In the carbonitride coating the interface between the white layer ϵ -Fe₃(CN) and diffusion zone of carbide/nitride α -Fe_(C-N) phases is more blurred [Fig. 12(b)]. Owing to the rapid cooling in the electrolyte flow, a primarily martensitic structure is observed here. An air-cooled carbide coating [Fig. 12(c)] has a thicker white layer and a thinner diffusion zone composed of cementite (ϵ -Fe₃C) and pearlite (α -Fe_(C) + ϵ -Fe₃C) respectively [39].

The temperature of the process is a very important

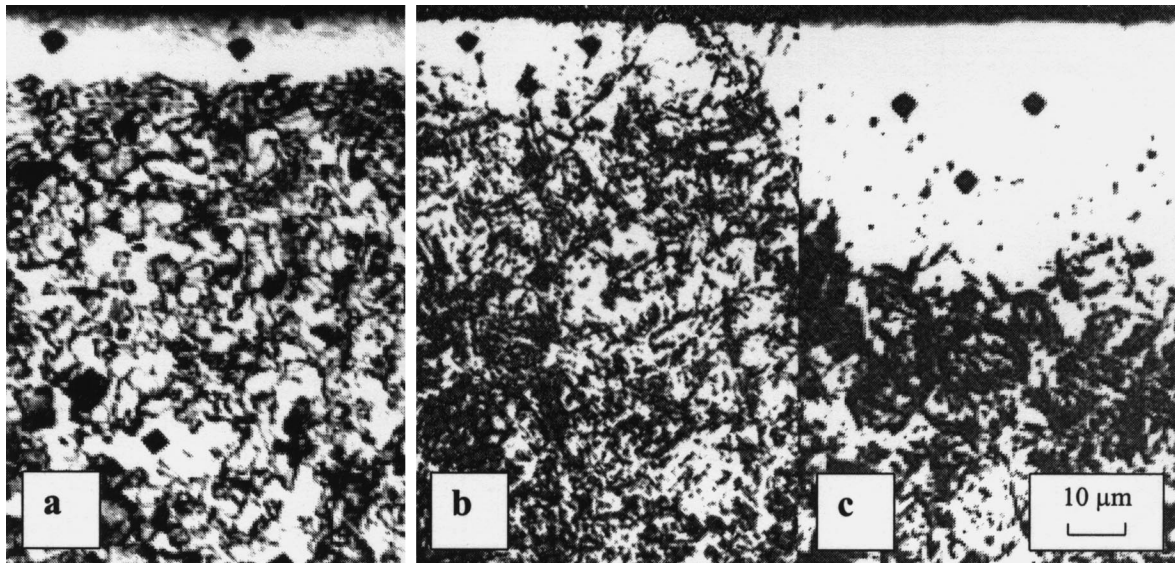


Fig. 12. Cross-section micrographs of 0.4C 1.0Cr steel surface layer after 4 min of treatments: (a) PEN at 640°C, (b) PEC/N at 800°C and (c) PEC at 860°C [39].

factor in achieving simultaneous saturation with both C and N. The concentration profiles of nitrogen and carbon in the outer surface and inner diffusion layers produced at either 670°C or 820°C have been studied previously in Ref. [51]. Layers of 100–150 μm thickness, and in some circumstances up to 200 μm thick, are formed in as little as 3 min. (Fig. 13). However, the elemental distribution through the layer is different in each case. At lower temperatures the diffusion of nitrogen gradually suppresses carbon take-up at the near surface. At 670°C an outer white layer with a thickness of 10–20 μm, containing 5 to 6% N and only 0.7% C is created, whereas the maximum amount of carbon (1.23%) is observed in the inner layer at a depth of 100 μm [Fig. 13(a)]. In contrast, the diffusion of carbon prevails over that of nitrogen at higher temperatures [Fig. 13(b)]. At 820°C this results in a reduction of the mean maximum nitrogen content to only 0.46%, with the mean maximum carbon content of 0.91%, now at the surface [Fig. 13(b)]. The microstructure of the outer and inner surface layers is transformed from a distinct compound (white) layer with an underlying diffusion zone into an extended diffusion layer only, formed predominantly of high carbon/nitrogen martensite.

5. Oxide coating performance

5.1. Mechanical properties

Oxide coatings can provide a considerable strengthening effect on aluminium substrates. This effect is displayed most clearly for sheet substrates, where a 100 to 200% rise in the effective Young's modulus has been

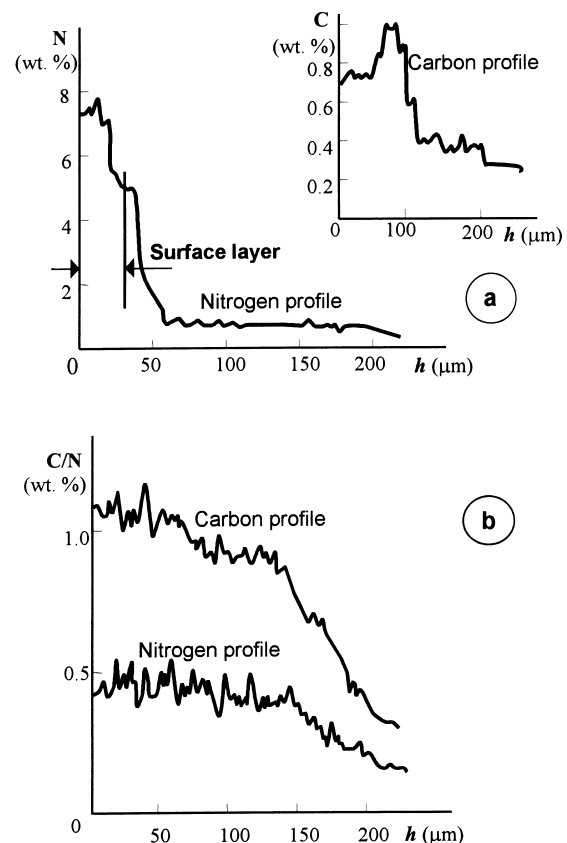


Fig. 13. Nitrogen and carbon profiles for low-carbon steel (SAE 1020) treated by the PEC/C process for 2 min at (a) 670°C and (b) 820°C [51].

observed [81]. This increase is dependent on the sheet thickness and the relative depth of the oxide layer.

The effective adhesion of the oxide layer, as evaluated

by microindentation tests [16,80,82], trends to increase with coating thickness. In 200 to 250 μm thick coatings the adhesion strength can reach 350 to 380 GPa, i.e. comparable to the tensile limit of the substrate in the case of aluminium. One explanation of the adhesion increase lies in a structural change in the coating's inner region due to diffusion processes. It is also likely that a thicker coating gives better load support, and that the interfacial region is, therefore, less stressed under the applied load.

Structural variations tend to create nonuniform hardness distributions through the oxide coating (Fig. 14.) The hardest zone is typically located at around 20 to 30 μm from the coating–substrate interface and relates to the maximum content of high temperature phases in the dense, inner coating region. Maximum hardness values correspond to 17 to 22 GPa for coatings based on α -alumina, 10 to 15 GPa for γ -phase coatings and 4 to 9 GPa for coatings based on mullite. In each case, the porous, outer regions of the coating possess lower hardness.

5.2. Tribological performance

5.2.1. Wear resistance

Films produced on aluminium alloys by the PEO technique show resistance to abrasive wear comparable to that of WC-based composites, boride diffusion coatings and corundum [78,83]. Fig. 15 illustrates the relative wear-resistance of various materials and coatings — showing the potential of PEO coatings.

The deterioration of PEO coatings under abrasive wheel tests with SiC powder of $\leq 70 \mu\text{m}$ size was studied in Ref. [84]. Taking into account the porosity variations and consequential nonuniform hardness distribution throughout the coating, the following steps of wear regimes can be distinguished, as indicated in Fig. 16:

1. a high wear rate of the outer layer (zone I, Fig. 16) is caused by the relatively low hardness and the porosity;

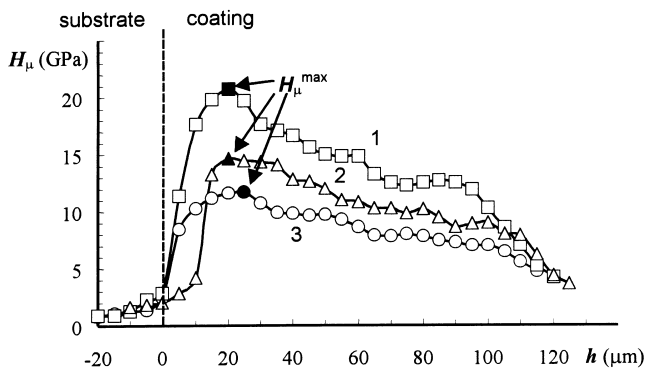


Fig. 14. Microhardness profiles through the oxide coatings based on (1) α -alumina, (2) γ -alumina and (3) mullite.

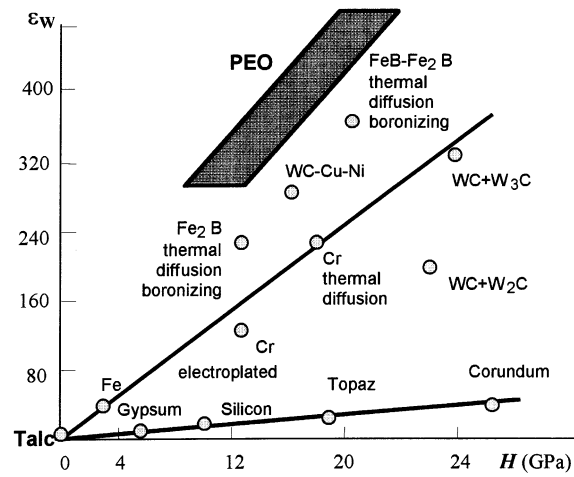


Fig. 15. Relative wear resistance (ϵ_w) diagrams for some materials in respect to a talc. H is material hardness [83].

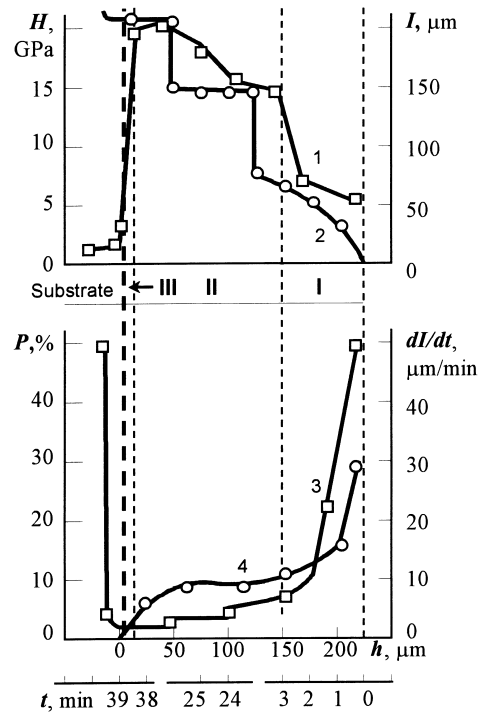


Fig. 16. (a) Wear variations I (1), hardness H (2) and wear rate dI/dt (3) versus time, and porosity P (4) through a PEO coating of thickness h ; the thickness of zone I (external/porous layer) is 30–60 μm , zone II (internal dense layer), 100–170 μm and zone III (diffusion layer), 3–5 μm [84].

2. the minimum wear rate in the inner region of the coating (zone II) is connected with the highest hardness and lowest porosity in this region;
3. the sharply increased wear rate at the coating–substrate interface (zone III) is due to the sudden reduction of hardness and load support as the soft, untreated aluminium substrate core is revealed.

The wear-resistance of components in corrosive environments can be improved by plasma electrolysis. For

example, good wear-resistance properties were found in an environment containing hydrocarbon and sulphuric compounds [76]. Here the wear mechanisms of the oxide layers differ from those of the metal. The processes of mechanical and corrosive deterioration of metals can occur simultaneously. In contrast, these processes can carry on separately on the oxide surface. The wear occurs in areas contacting with a counter-body, whereas the corrosion takes place in the pores of the oxide layer.

5.2.2. Frictional behaviour

5.2.2.1. Lubricated friction The frictional performance of oxide coatings under lubricated conditions has been studied both for oil and water environments. A reduction in the friction coefficient for oxide-steel pairs to $\mu \approx 0.015$ from typically 0.4 for a steel-on-steel contacts has been recorded when the (porous) oxide film was impregnated with oil [84].

Block-on-disc friction characteristics of PEO coatings on aluminium alloys against each other have been studied in industrial water and seawater environments [78,84]. It has been stated that a combined pairing of α - Al_2O_3 -based coatings showed $\mu = 0.023$ to 0.025 at pressures up to 16 MPa. Coating pairs based on γ - Al_2O_3 gave $\mu = 0.005$ to 0.008 up to a critical pressure of 8 MPa. Friction pairs based on mullite coatings can accommodate a critical pressure up to 4 MPa.

5.2.2.2. Unlubricated friction The frictional behaviour of aluminium oxide coatings under dry conditions has also been studied [80,85]. Pin-on-disc tests against Al_2O_3 , steel and WC-Co ball counterface materials have been performed in vacuum, under nitrogen and in air with controlled humidity. The results shown in Fig. 17 can be explained taking into account both mechanical and chemical components of the friction contact. The friction coefficients of contacting materials with similar mechanical properties, such as oxide coatings against Al_2O_3 or the coating against itself, are defined primarily by tribo-chemical interactions between the contacting faces. These interactions are strongly dependent on the

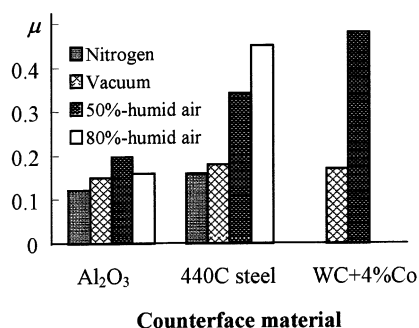


Fig. 17. Pin-on-disc friction characteristics of PEO coatings against different materials in various environments [80,85].

composition of the external environment. Thus, for example, raising air humidity to 80% promotes formation of a thin lubricating film of aluminium hydroxide, which results in a reduction of friction coefficient.

The friction of materials with different mechanical properties, such as oxide coatings against steel and WC-Co, is accompanied by continual renovation of the friction contact area. Owing to this, the chemical interaction is accelerated in the contacting area, resulting in a rise in friction coefficient. To reduce dry friction in such pairs the deposition of thin carbon films on top of the oxide coating has been considered [86]. This achieves a reduction in friction coefficient from 0.49–0.62 to 0.17–0.32 against a WC-Co ball counterface.

Recent investigations [87] indicate that the overall thickness of the oxide coating can itself have a strong influence on mechanical properties, depending on the contact regime. In terms of overall tribological performance, thick PEO coatings appear to perform best in sliding, scratch and impact tests, whereas thin coatings can also be surprisingly effective in both impact and low-load sliding wear. PEO coatings of intermediate thickness provided relatively poor performance in all of the tribological tests performed [87]. There is obviously considerable scope to adjust the microstructure and composition of these coatings, as well as the thickness, to optimise performance for particular contact conditions. Considering the excellent load-support characteristics of PEO alumina coatings, there are also many prospects for the development of novel multilayered and hybrid/duplex coating structures for protection of aluminium, e.g on the basis of a PEO coating as a precursor to PVD (or other) coating deposition processes.

5.3. Heat resistance

Since alumina and silica both have high melting points, good heat-protective properties from such oxide coatings might be expected. However, the thermal expansion coefficient of these layers differs substantially from those of the substrate material (by up to a factor of ten). Nevertheless, coatings produced, for example, in concentrated silicate electrolytes can successfully resist significant external heat fluxes without adhesion damage — due in part to their high porosity [41].

5.4. Dielectric properties

The high electrical resistance and breakdown strength of silica and alumina provide strong dielectric properties in PEO coatings. These properties were evaluated in Refs. [88,89], where values of specific resistance from 2.7×10^{14} to $3.5 \times 10^{13} \Omega \text{ m}$ were obtained. Coatings produced in solutions of 1 to 5% dissolved silicate possess the best properties in this respect.

Electrical resistivity is also a factor in plasma electrol-

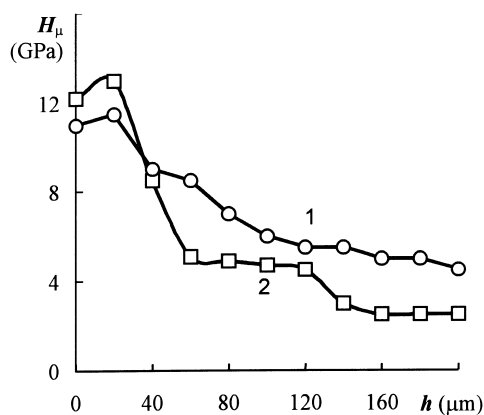


Fig. 18. Typical hardness profiles for SAE 1020 treated by PEC/PEN for 3 min at (1) 250 V and (2) 220 V [51].

ysis. This is reduced when the process transfers to the arc discharge regime and then remains constant independent of the oxidation time. Although the properties are less good than sodium glass [41], these coatings can be used as a low-voltage dielectric material if the appropriate treatment route is chosen.

6. The performance of nitride/carbide surface layers

6.1. Microhardness

The mechanical performance of nitride/carbide surface layers was evaluated on SAE 1020 steel, after a PEN/C treatment of 3-min duration in an electrolyte composed of $\text{HCONH}_2 + 8\%$ ($\text{KCl} + \text{H}_2\text{O}$) [51]. Applied negative potentials of 220 V and 250 V created surface temperatures of 670°C and 820°C respectively. Typical hardness profiles for these saturated layers are shown in Fig. 18. The hardness of the outermost surface layer is reduced with increasing electrode voltage, corresponding to a change in surface microstructure from an iron-nitride ‘white’ layer to an extended iron-carbon-nitro-

gen diffusion layer. The high surface hardness (HV1300) is followed by an abrupt decrease at a certain depth (i.e. below the ‘white’ nitride layer) for the specimen treated at 220 V. The gradient of the hardness decrease is, however, more shallow for the specimen treated at 250 V.

6.2. Friction and wear properties

The high hardness of surface layers produced by PES creates the possibility for improvement of friction and wear properties of many materials, but steels are the obvious candidates. Abrasive wear was studied for a stainless steel (0.2% C, 13% Cr) comparing conventional thermal hardening and PEN at 620°C in an electrolyte containing ammonium chloride and nitric acid [90]. An increase in wear resistance of 15–20% was noted for the samples subjected to the nitrogen-saturation treatment. The effect of the PEN regimes on the tribological performance of nitride layers on a medium carbon steel (0.4% C, 1.0% Cr) was studied in more detail in Ref. [91]. When produced in the same electrolyte, the layers had a thickness up to 0.5 mm and a hardness of 6 to 9 GPa. The hardest layers were obtained at 700–750°C and consisted of a 30 μm outer ‘white’ nitride layer and an inner diffusion zone of high-nitrogen martensite. The friction characteristics of these layers in unlubricated pin-on-disc sliding against sintered TiC (29 GPa hardness) are summarised in Table 4, with some other materials/treatments for comparison. The results show that although friction coefficients μ of the PEN layers were not the lowest, they do however provide the lowest wear rates I and temperatures in the contact area T_{cont} .

The relative wear resistance of N/C layers on SAE 1020 steel was studied in Ref. [51]. The linear wear rate was compared for specimens before and after plasma electrolytic treatment. The results also showed that the treated specimens had much better wear resistance.

Table 4
Comparative tribological characteristics^a of nitride layers steels [90]

Treatment regime			H_μ (GPa)	Friction characteristics		
Electrolyte	T (°C)	τ (min)		μ	I (μm/min)	T_{cont} (°C)
<i>Medium carbon steel (0.4% C, 1% Cr)</i>						
Without treatment			2–2.5	0.42	270	120
NH_4Cl , 11%; HNO_3 , 5%	750	5	8.5–9	0.34	18	70
NH_4Cl , 11%; HNO_3 , 11%	750	5	9	0.25	22	70
		2	8.5–9	0.25	20	70
<i>Tool steel (1% C, 1.5% W, 1% Mn, 1% Cr)</i>						
Thermal diffusion boronizing			3–4	0.3	40	140
Thermal hardening			7–8	0.2	32	100

^a At 3.0 MPa loading and 1.25 m/min sliding speed.

6.3. Corrosion performance

The corrosion behaviour of SAE 1020 specimens PEN/C treated for 3 min at 220 V was also assessed [51]. The specimens were immersed in a 0.1 N sulphuric acid solution for 10 min and then an AC voltage was applied. A comparison of the values of corrosion resistance indicated that the corrosion resistance was approximately 30 times higher for the treated SAE 1020 steel sample than that for the untreated one. Similar improvements were also observed for other ferrous alloy materials.

7. Possible applications

Various programmes have been undertaken to promote the industrial application of plasma electrolysis techniques during the last decade. A summary of the applications reported so far is given in Table 5.

The data in Table 5 demonstrate that PEO coatings can successfully compete with anodising and thermal oxidation techniques, as well as provide an inexpensive, low-weight alternative to certain 'difficult' (in terms of manufacture and processing) materials, in a wide range of industries. The excellent wear, friction, corrosion and thermal properties of these coatings are of particular interest in textile machines, aerospace components and gas/oil extraction and refining machinery.

Because of the relatively simple equipment required, high treatment efficiencies and the possibility of continuous treatment of workpieces, methods based on PES also show considerable promise for practical industrial applications. Hard, corrosion-resistant and thermally stable layers of borides, nitrides or carbides can be produced on various metal surfaces. Large-area workpieces, which are difficult to treat in a chamber process, can easily be accommodated. Furthermore, PES methods can be utilised as pretreatments in duplex processes involving electroplating, PVD, or other coatings. For example, thin, hard PVD coatings can be deposited onto a thick diffusion layer fabricated by PEN/C to provide good adhesion and load support on low-alloy substrates. The PES technology is also potentially beneficial for some metals as a precursor to depositing diamond or diamond-like coatings. Furthermore, the technique can also be used as an alternative to conventional induction hardening, owing to its characteristic of rapid heating, which can be used to create a high temperature difference between the substrate surface and the interior.

8. Summary and conclusions

The PED methods described in this paper have become available due to the propagation of conventional

electrolysis processes into the field of high-energy ionised plasma/arcs. At potentials exceeding some critical value (U_2 or U_5 from Fig. 2) a variety of electrical discharge phenomena active in the near-electrode area can be employed to alter the morphology of the electrode–electrolyte interface and control the treatment processes occurring. Plasma discharges enhance heating and diffusion processes, cataphoretic effects and plasma thermochemical reactions at the electrode surface. Depending on the electrolyte composition and electrode polarity, many processes, including those of PEO and PES, can be applied.

PEO is a technique that operates at potentials above the breakdown voltage of an oxide film growing on the surface of a passivated metal anode and is characterised by multiple arcs moving rapidly over the treated surface. Complex compounds can be synthesised inside the high voltage breakthrough channels formed across the growing oxide layer. These compounds are composed of oxides of both the substrate material (typically aluminium) and electrolyte-borne modifying elements (e.g. silicon). Plasma thermochemical interactions in the multiple surface discharges result in a coating growing in both directions from the substrate surface. Although local temperatures are instantaneously extremely high, normally the bulk substrate temperature is below 100°C. At a particular combination of electrolyte composition and current regime the discharge modifies the microstructure and phase composition of the substrate from metal alloy to complex ceramic oxide. As a result, thick wear-resistant layers (maximum hardness 18 to 23 GPa and maximum thickness about 500 µm) with excellent adhesion can be achieved on aluminium alloy components, and the production cost is competitive with that of conventional anodising processes.

PES is carried out at potentials above the breakdown voltage of the gas bubbles formed on the surface of the workpiece, which in this case may be either cathodic or anodic with respect to the electrolyte. At some critical voltage the vapourised electrolyte and/or gas released by oxidation/reduction processes on the electrode surface forms a continuous vapour envelope around the electrode, in which an arc-plasma is established providing reactive elements for substrate treatment. Because of the much larger current density achieved in such atmospheric discharges, compared with conventional vacuum plasma treatments, intense ion bombardment on the surface of the workpiece can occur, thus causing rapid heating and enhanced activation of the substrate surface. Therefore, only short treatment times (3–5 min) are required for fabrication of 200–500 µm thick diffusion/saturation layers, which have good mechanical and corrosion properties. Various compounds, such as nitrides, carbides and borides, can be formed in an appropriately selected electrolyte.

The potential of the new plasma electrolytic coating

Table 5
Applications and characteristic properties in the PED techniques

Field of application	Material/treatment to be substituted		Advanced material/treatment		Characteristics of effectiveness	
	Component	Substrate	Coating	Technical	Economical	
<i>Textile machine building/</i> Spinning & winding frames, looms, pattern cutting machines	Rotors, needle casing elements	High strength Al-alloy/ deep anodising	α -Al ₂ O ₃ , 100–150 μ m, 15–18 GPa	200–300% increased lifetime, reduced thread fluffiness	60–80% reduced production cost	
	Winding drums, rolls Shuttle cases	Steel/Cr electroplating	B ₄ C, 100–150 μ m, 4–5 GPa	200–300% increased lifetime, 100–200% reduced friction	Production time & cost reduced by 80% and 20–30% respectively	
	Cutting knives	Tool steel/ hardening	γ -Al ₂ O ₃ , 60–120 μ m, 10–14 GPa	150–200% increased lifetime, weight and inertial force reduction	50–60% reduced production cost	
<i>Gas- and oil- industry/</i> Gear-, rotary-, immersed-pumps; locking fittings and valves	Operating wheels, sealing rings	Stainless steel, cast iron		10–20% increased lifetime, absence of cracking	70% reduced production cost	
	Locking disks and spheres	Sintered ceramics		Improved heat exchange	60% reduced production cost	
<i>Engine industry/diesel-, gasoline- & electric engines</i>	Cases	Al-alloy/coloured anodising	γ -Al ₂ O ₃ , 60–120 μ m, 10–14 GPa	160–250% increased lifetime, reduction of fuel consumption	Up to 80% reduced production cost	
	Pistons	Al-Si alloys/ depth anodising	Mullite, 100–150 μ m, 6–10 GPa			
<i>Electrical engineering & electronics/</i> Electrolytic capacitors, heat sinks	Cylinder liners	High strength cast iron				
	Electrode foils	Al/anodising	γ -Al ₂ O ₃ , 30–50 μ m	20–50% increased capacity	Up to 80% reduced oxidation time	
	Heat sinks	Al-alloy/ coloured anodising		Improved heat exchange	Up to 60% reduced production cost	
<i>Biomedical industry/</i> Mixers, prostheses	Blades	Stainless steel	α -Al ₂ O ₃ , 120–160 μ m, 14–18 GPa	160–250% increased lifetime	Up to 70% reduced production cost	
	Implants, endo- prostheses	Ti	TiO ₂ , 4–10 μ m	Improved bio-compatibility	N.A.	
<i>Vacuum engineering/</i> Turbo-molecular pumps, evaporators	Rotors, stators, wheels	Stainless steel	γ -Al ₂ O ₃ , 50 μ m, 14 GPa	200% increased lifetime, reduced vibration	About 80% reduced production cost	
	Boats	W, Mo, C, B, Ta	α -Al ₂ O ₃ , 160–200 μ m; SiO ₂ , 400–600 μ m	50–300% increased lifetime	reduced production cost	
<i>Air & space industry/</i> Gears, optical-devices	Gears, wheels	Stainless steel	γ -Al ₂ O ₃ , 60–120 μ m, 10–14 GPa	Up to 100% increased lifetime, weight reduction	60% reduced production cost	
	Cases	Ti/thermal oxidation	TiO ₂ , 4–10 μ m	Higher heat absorptency, and emission	N.A.	
<i>Vessel building industry/</i> Vessel pipework and devices	Pipes, fittings, device cases	Ti/PEO	TiO ₂ , 4–10 μ m	Increased corrosion resistance	Up to 90% reduced production time	
	Screw		Al ₂ TiO ₅ , 50–100 μ m, 4–6 GPa	20–30% reduced friction		
<i>Tool industry/Cutting & pressing tools</i>	Cutting tools, drills, mills	High speed steel/ hardening	α -WB, W ₂ B ₅ , B ₄ C, 100–150 μ m, 4–5 GPa	50–150% increased lifetime	Production time & cost reduced by 70% & 20–30% respectively	
	Pressing moulds, Mixer, carbonising/	Tool steel/ hardening	ϵ -Fe ₃ (CN), γ , (γ' + θ), 300–450 μ m, 4–5 GPa	50–150% increased lifetime	60% reduced production cost	

and treatment processes described above is clearly considerable. They can be expected to be useful in an ever widening range of applications, particularly in view of an increasing drive for the use of weight-saving or high strength-to-weight ratio materials. Furthermore, these methods are likely to be used as precursor treatments in combination with other coating methods, to provide 'hybrid' or 'duplex' processes, which can extend the capabilities of both plasma electrolysis and other coating techniques.

Acknowledgement

Partial funding support for A.L. Yerokhin in this work was provided by Ion Coat Ltd. and is acknowledged with thanks.

References

- [1] N.P. Sluginov, J. Russ. Phys. Chem. Soc., 12 1–2 Phys. (1880) 193, in Russian.
- [2] A. Günterschultze, H. Betz, *Electrolytkondensatoren*, Krayn, Berlin, 1937.
- [3] W. McNiell, G.F. Nordbloom, US Patent 2854 390, September 30, 1958.
- [4] W. McNiell, L.L. Gruss, US Patent 3293 158, 1966.
- [5] G.A. Markov, G.V. Markova, USSR Patent 526 961, Bul. Inv. 32, 1976.
- [6] A.V. Nikolaev, G.A. Markov, B.I. Peshchevitskij, *Izv. SO AN SSSR. Ser. Khim. Nauk* 5 (12) (1977) 32, in Russian.
- [7] G.A. Markov, V.V. Tatarchuk, M.K. Mironova, *Izv. SO AN SSSR. Ser. Khim. Nauk* 3 (7) (1983) 34, in Russian.
- [8] L.A. Snezhko, L.A. Beskrovnyj, Yu.M. Nevkrytyj, V.I. Tchernenko, *Zashch. Met.* 16 (3) (1980) 365, in Russian.
- [9] L.A. Snezhko, G.V. Rozenboym, V.I. Tchernenko, *Zashch. Met.* 17 (5) (1981) 618, in Russian.
- [10] L.A. Snezhko, V.I. Tchernenko, *Elektron. Obrab. Mater.* (2) (1983) 25, in Russian.
- [11] L.A. Snezhko, V.I. Tchernenko, *Elektron. Obrab. Mater.* (4) (1983) 38, in Russian.
- [12] V.I. Tchernenko, L.A. Snezhko, C.B. Tchernova, *Zashch. Met.* 20 (3) (1984) 454, in Russian.
- [13] L.A. Snezhko, S.G. Pavlva, V.I. Tchernenko, *Zashch. Met.* 20 (4) (1984) 292, in Russian.
- [14] G.A. Markov, M.K. Mironova, O.G. Potapova, *Izv. AN SSSR. Ser. Neorgan. Mater.* 19 (7) (1983) 1110, in Russian.
- [15] A.A. Petrosyants, V.N. Malyshev, V.A. Fyedorov, G.A. Markov, *Trenie Iznos* 5 (2) (1984) 350, in Russian.
- [16] V.N. Malyshev, S.I. Bulychov, G.A. Markov, V.A. Fyedorov, A.A. Petrosyants, V.V. Kudinov, M.H. Shorshorov, *Fiz. Khim. Obrab. Mater.* (1) (1985) 82, in Russian.
- [17] V.A. Fyedorov, V.V. Belozorov, N.D. Velikosel'skaya, S.I. Bulychov, *Fiz. Khim. Obrab. Materialov* 4 (1988) 92, in Russian.
- [18] V.S. Rudnev, P.S. Gordienko, preprint no. 3384-B87, Inst. Khimii DVO AN SSSR, Vladivostok, 1987, in Russian.
- [19] O.A. Khrisanfova, P.S. Gordienko, preprint no. 2986-B89, Inst. Khimii DVO AN SSSR, Vladivostok, 1987, in Russian.
- [20] P.S. Gordienko, P.M. Nedorozov, L.M. Volkova, T.P. Yarovaya, O.A. Khrisanfova, *Zashch. Met.* 25 (1) (1989) 125, in Russian.
- [21] P. Kurze, W. Krysmann, G. Marx, Z. Wiss, Tech. Hochsch. Karl-Marx-Stadt 24 (1982) 139.
- [22] K.H. Dittrich, W. Krysmann, P. Kurze, H.G. Schneider, *Cryst. Res. Technol.* 19 (1) (1984) 93.
- [23] W. Krysmann, P. Kurze, K.H. Dittrich, H.G. Schneider, *Cryst. Res. Technol.* 19 (7) (1984) 973.
- [24] P. Kurze, J. Schreckenbach, T. Schwarz, W. Krysmann, *Metallob-erflaeche* 40 (12) (1986) 539.
- [25] L.S. Saakian, A.P. Yefremov, L.Y. Ropyak, A.V. Apelfeld, *Corrosion Control and Environment Protection. Informative survey*, VNIOENG, Moscow, (6), 1986, in Russian.
- [26] V.A. Fyedorov, A.G. Kan, R.P. Maksutov, *Surface Strengthening of Oil & Gas Trade Facilities by Micro Arc Oxidation*, VNIOENG, Moscow, (6) 1989, in Russian.
- [27] G.A. Markov, B.S. Gizatullin, I.B. Rychazhkova, USSR Patent 926083, Bul. Inv. 17, 1982.
- [28] L.A. Snezhko, V.I. Tchernenko, USSR Patent 973 583, Bul. Inv. 23, 1982.
- [29] P. Kurze, W. Krysmann, G. Marx, K.H. Dittrich, DDR Patent DD-WP C25 D/236 988(5).
- [30] R.J. Gradkovsky, S.N. Bayles, US Patent 3 956 080, May 11, 1974.
- [31] S.D. Brown, K.J. Kuna, T.B. Van, *J. Am. Ceram. Soc.* 54 (8) (1971) 384.
- [32] T.B. Van, S.D. Brown, G.P. Wirtz, *Am. Ceram. Soc. Bull.* 56 (6) (1977) 563.
- [33] W. Xue, Z. Deng, Y. Lai, R. Chen, *J. Am. Ceram. Soc.* 81 (1998) 1365.
- [34] B.R. Lazarenko, N.I. Lazarenko, *Electric Spark Treatment of Metals*, Gosenergoizdat, Moscow, 1950.
- [35] B.R. Lazarenko, N.I. Lazarenko, *Elektron. Obrab. Mater.* (1) (1966) 3, in Russian.
- [36] B.R. Lazarenko, P.N. Belkin, A.A. Faktorovich, *Elektron. Obrab. Mater.* (6) (1975) 31, in Russian.
- [37] V.N. Duradzy, I.V. Bryantsev, *Elektron. Obrab. Mater.* (1) (1977) 45, in Russian.
- [38] V.N. Duradzy, G.A. Fornya, *Elektron. Obrab. Mater.* (4) (1988) 30, in Russian.
- [39] V.N. Duradzy, A.S. Parsadanyan, *Metal Heating in Electrolytic Plasma*, Shtiintsa, Kishinev, 1988, in Russian.
- [40] V.N. Duradzy, N.A. Polotebnova, *Elektron. Obrab. Mater.* (1) (1984) 83, in Russian.
- [41] V.I. Tchernenko, L.A. Snezhko, I.I. Papanova, *Coatings by Anodic Spark Electrolysis*, Khimiya, Leningrad, 1991, in Russian.
- [42] S. Ikonopisov, *Electrochim. Acta* 22 (10) (1977) 1077.
- [43] J. Monterro, M. Fernandez, J.M. Albella, *Electrochim. Acta* 32 (1) (1987) 171.
- [44] A.V. Apelfeld, V.B. Lyudin, B.V. Kharitov, P.H. Alymov, *Proceedings of the Russian Conference 'New Materials & Technology'*, MGATU, Moscow, 1994, in Russian.
- [45] A.V. Timoshenko, Yu.V. Magurova, *Zashch. Met.* 31 (5) (1995) 523, in Russian.
- [46] G.A. Markov, Ye.K. Shulepko, *Zashch. Met.* 31 (6) (1995) 643, in Russian.
- [47] G.A. Markov, O.P. Terleeva, Ye.K. Shulepko, I.M. Gubkin *MINKh&GP Collection of Works vol. 185*, MINKh&GP, Moscow, 1985, p. 54, in Russian.
- [48] K.A. Naugil'nykh, N.A. Roy, *Electric Discharges in Water*, Nauka, Moscow, 1971, in Russian.
- [49] D.Yu. Kharitonov, E.I. Gutsevich, G.I. Novikov, A.A. Fridman, *On Mechanism of Pulsed Electrolytic Spark Oxidation in Saturated Sulfuric Acid*, TsNIIAtomInform, Moscow, 1988, in Russian.
- [50] G.I. Skanavi, *Physics of Dielectrics. Strong Fields*, Izdatelstvo Fiz.-Mat. Literaturny, Moscow, 1958, in Russian.
- [51] X. Nie, Q.K. Hao, J.M. Wei, *J. Wuhan Univ. Technol.* 11 (1) (1996) 28.

- [52] S.S. Kutateladze, Fundamentals of Heat Exchange Theory, Atom-Izdat, Moscow, 1979, in Russian.
- [53] Ya.F. Kolodin, Svar. Proizvod. 2 (1975) 15, in Russian.
- [54] A.Ya. Zanin, P.M. Kovakenko, M.I. Serdyuk, Y.I. Nazareko, Electron. Obrab. Mater. (4) (1983) 85, in Russian.
- [55] V.N. Duradgy, I.N. Morar, L.A. Polotebnova, L.V. Kiseleva, Electron. Obrab. Mater. (1) (1986) 49, in Russian.
- [56] V.N. Duradgy, I.V. Bryantsev, A.M. Mokrova, T.S. Lavrova, Electron. Obrab. Mater. (6) (1979) 20, in Russian.
- [57] B.R. Lazarenko, Y.M. Lakhin, A.A. Faktorovich, V.N. Duradzi, I.V. Bryantsv, in: G.N. Dubinin, Y.D. Kogan (Eds.), Advanced Techniques of Thermal Chemical Treatment, Mashinostrojenie, Moscow, 1979, in Russian.
- [58] S.Ye. Kuzenkov, B.P. Saushkin, Electron. Obrab. Mater. (4) (1997) 27, in Russian.
- [59] V.V. Bakovets, O.P. Dolgovesova, I.P. Polyakova, Plasma Electrolytic Anode Treatment of Metals, Nauka, Novosibirsk, 1991, in Russian.
- [60] K. Fetter, M.Ya. Kolotyrykin, Trans. from German, Electrochemical Kinetics, Khimiya, Leningrad, 1967, in Russian.
- [61] A.L. Yerokhin, Electrophysical & Electrochemical Treatment of Materials, TulGU, Tula, 1996, p. 30, in Russian.
- [62] S.Ye. Kuzenkov, B.P. Saushkin, Proceedings of the Russian Conference SET'97, Tula, June 3–4 (1997) 327, Tula State University, in Russian.
- [63] N.M. Gegechkori, Sov. J. Exp. Tech. Phys. 21 (4) (1951) 493, in Russian.
- [64] V.A. Fyedorov, B.B. Belozarov, N.D. Velikoselskaya, Fiz. Khim. Obrab. Mater. (1) (1991) 87 in Russian.
- [65] P.S. Gordienko, S.V. Gnedenkov, Micro Arc Oxidation of Titanium and its Alloys, Dalnauka, Vladivostok, 1997, in Russian.
- [66] P.S. Gordienko, Coating Formation on Anodically Polarised Electrodes at the Potentials of Sparking and Breakdown, Dalnauka, Vladivostok, 1996, in Russian.
- [67] A.L. Yerokhin, V.V. Lyubimov, R.V. Ashitkov, Fiz. Khim. Obrab. Mater. (5) (1996) 39, in Russian.
- [68] A.L. Yerokhin, V.V. Lyubimov, R.V. Ashitkov, Ceram. Int. 24 (1) (1998) 1.
- [69] R.R. Nevyantseva, T.M. Timergazina, Proceed of the Russian Conf. SET'97, Tula, June 3–4, (1997) 267, Tula State University, in Russian.
- [70] G.A. Markov, E.K. Shulepko, O.P. Terleeva, V.N. Kirillov, V.A. Fyedorov, A.G. Kann, R.A. Maksutov, V.N. Glazunov, USSR Patent 1 339 818, Bul. Inv. 35, 1985.
- [71] G.A. Markov, E.K. Shulepko, O.P. Terleeva, V.N. Kirillov, USSR Patent 1 451 821, BI Bul. Inv. 2, 1989.
- [72] A.L. Yerokhin, V.V. Lyubimov, A.N. Ryzhov, Electrochemical & Electrophysical Treatment of Materials, TulGTU, Tula, 1993, p. 5, in Russian.
- [73] G.A. Markov, V.I. Belevantsev, O.P. Terleeva, E.K. Shulepko, A.I. Slonova, Vestn. MGTU Ser. Mashinostr. 1 (1992) 34, in Russian.
- [74] V.S. Rudnev, P.S. Gordiyenko, Zashch. Met. 29 (2) (1993) 304, in Russian.
- [75] A.V. Timoshenko, S. Gut, B.K. Opara, K. Pshibylovich, Y.V. Magurova, Zashch. Met. 30 (2) (1994) 175, in Russian.
- [76] L.S. Saakiyan, A.P. Efremov, I.A. Soboleva, Zashch. Met. 30 (1) (1994) 101, in Russian.
- [77] A.L. Yerokhin, V.V. Lyubimov, A.A. Voevodin, Proceedings of International Conference on Advanced & Laser Technology 'ALT'92' (2) (1992) 52, Institute of General Physics of the Russian Academy of Science, Moscow, 1992.
- [78] V.A. Fyedorov, Doctor of Sci. Thesis, GANG, Moscow, 1993 (in Russian).
- [79] A.A. Voevodin, A.L. Yerokhin, V.V. Lyubimov, M.S. Donley, J.S. Zabinski, Surf. Coat. Technol. 86–87 (1996) 516.
- [80] A.L. Yerokhin, A.A. Voevodin, V.V. Lyubimov, J.S. Zabinski, M.S. Donley, Surf. Coat. Technol. 110 (3) (1998) 140.
- [81] V.N. Malyshev, N.V. Malysheva, Proceedings of Russian Conference 'Anode'88', KAI, Kazan, 1988, p. 88, in Russian.
- [82] S.I. Bulychev, V.P. Alekhin, Materials Testing by Continuous Indentation, Mashinostroenie, Moscow, 1990, in Russian.
- [83] V.A. Fyedorov, I.M. Gubkin MINKh&GP Collection of Works vol. 185, MINKh&GP, Moscow, 1985, p. 22, in Russian.
- [84] V.N. Malyshev, A.A. Petrosyants, I.M. Gubkin MINKh&GP Collection of Works vol. 185, MINKh&GP, Moscow, 1985, p. 39, in Russian.
- [85] A.L. Yerokhin, V.V. Lyubimov, A.A. Voevodin, M.S. Donley, J.S. Zabinski, Proceedings of the Russian Conference SET'97, Tula, June 3–4 (1997) 239, Institute of General Physics of the Russian Academy of Science, Moscow, 1992, in Russian.
- [86] A.L. Yerokhin, A. Matthews, S. Dowey, V.V. Lyubimov, Trenie i Iznos 19 (5) (1998) 642, in Russian.
- [87] X. Nie, A. Leyland, A.L. Yerokhin, H.W. Song, S. Dowey, A. Matthews, Surf. Coat. Technol. (1999) in press.
- [88] V.V. Bakovets, I.P. Dolgovesova, G.L. Nikiforova, Zashch. Met. 22 (3) (1986) 440, in Russian.
- [89] S.G. Pavlyus, V.I. Sobornitski, Yu.A. Sheprut, L.A. Snezhko, V.I. Tchernenko, Elektron. Obrab. Mater. (3) (1987) 34, in Russian.
- [90] Ye.A. Pasinkovsky, I.M. Goldman, R.P. Sorokina, Electron. Obrab. Mater. (2) (1976) 86, in Russian.
- [91] P.N. Belkin, Ye.A. Pasinkovsky, Yu.G. Tkachenko, A.A. Faktorovich, V.K. Yulyugin, Electron. Obrab. Mater. (4) (1981) 43, in Russian.